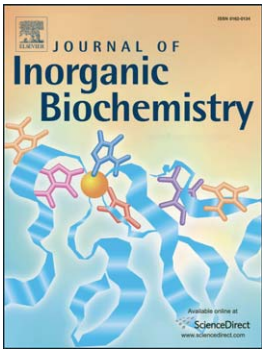

Induction of apoptosis in leukemia cell lines by new copper(II) complexes containing naphthyl groups *via* interaction with death receptors

Christiane Fernandes, Adolfo Horn Jr, Bruna F. Lopes, Erika S. Bull, Nathália F.B. Azeredo, Milton M. Kanashiro, Franz V. Borges, Adailton J. Bortoluzzi, Bruno Szpoganicz, Anderson B. Pires, Roberto W.A. Franco, João Carlos de A. Almeida, Leide L.F. Maciel, Jackson A.L.C. Resende, Gerhard Schenk

PII: S0162-0134(15)30087-8
DOI: doi: 10.1016/j.jinorgbio.2015.09.014
Reference: JIB 9815

To appear in: *Journal of Inorganic Biochemistry*

Received date: 28 May 2015
Revised date: 10 September 2015
Accepted date: 30 September 2015

Please cite this article as: Christiane Fernandes, Adolfo Horn Jr, Bruna F. Lopes, Erika S. Bull, Nathália F.B. Azeredo, Milton M. Kanashiro, Franz V. Borges, Adailton J. Bortoluzzi, Bruno Szpoganicz, Anderson B. Pires, Roberto W.A. Franco, João Carlos de A. Almeida, Leide L.F. Maciel, Jackson A.L.C. Resende, Gerhard Schenk, Induction of apoptosis in leukemia cell lines by new copper(II) complexes containing naphthyl groups *via* interaction with death receptors, *Journal of Inorganic Biochemistry* (2015), doi: 10.1016/j.jinorgbio.2015.09.014

Induction of apoptosis in leukemia cell lines by new copper(II) complexes containing naphthyl groups *via* interaction with death receptors

Christiane Fernandes [a,*], Adolfo Horn Jr [a,*], Bruna F. Lopes [a], Erika S. Bull [a], Nathália F. B. Azeredo [a], Milton M. Kanashiro [b], Franz V. Borges [b], Adailton J. Bortoluzzi [c], Bruno Szpoganicz [c], Anderson B. Pires [c], Roberto W. A. Franco [d], João Carlos de A. Almeida [e], Leide L. F. Maciel [e], Jackson A. L. C. Resende [f] and Gerhard Schenk [g]

[a] *Laboratório de Ciências Químicas, Universidade Estadual do Norte Fluminense, 28013-602, Campos dos Goytacazes/RJ, Brazil*

[b] *Laboratório de Biologia do Reconhecer, Universidade Estadual do Norte Fluminense, 28013-602, Campos dos Goytacazes/RJ, Brazil*

[c] *Departamento de Química, Universidade Federal de Santa Catarina, 88040-900, Florianópolis/SC, Brazil*

[d] *Laboratório de Ciências Físicas, Universidade Estadual do Norte Fluminense, 28013-602, Campos dos Goytacazes/RJ, Brazil*

[e] *Laboratório de Fisiologia e Bioquímica de Microrganismos, Universidade Estadual do Norte Fluminense Darcy Ribeiro, 28013-602, Campos dos Goytacazes/RJ, Brazil*

[f] *Laboratório de Difração de Raios X, Universidade Federal Fluminense, 24020-150, Niterói/RJ, Brazil*

[g] *School of Chemistry and Molecular Biosciences, The University of Queensland, Brisbane, QLD 4072, Australia*

Dedicated to Prof. Graeme R. Hanson *in memoriam.*

*corresponding authors. E-mail: chrisf@uenf.br (C. Fernandes), adolfo@uenf.br (A. Horn Jr).

ABSTRACT: The synthesis, physico-chemical characterization and cytotoxicity of four new ligands and their respective copper(II) complexes toward two human leukemia cell lines (THP-1 and U937) are reported (*i.e.* [(HL1)Cu(μ-Cl)$_2$Cu(HL1)]Cl$_2$. H$_2$O **(1),** [(H2L2)Cu(μ-Cl)$_2$Cu(H2L2)]Cl$_2$.5H$_2$O **(2),** [(HL3)Cu(μ-Cl)$_2$Cu(HL3)]Cl$_2$.4H$_2$O **(3),** [(H2L4)Cu(μ-Cl)$_2$Cu(H2L4)]Cl$_2$.6H$_2$O **(4)**). Ligands HL1 and HL3 contain two pyridines, amine and alcohol moieties with a naphthyl pendant unit yielding a N3O coordination metal environment. Ligands H2L2 and H2L4 have pyridine, phenol, amine and alcohol groups with a naphthyl pendant unit providing a N2O2 coordination metal environment. These compounds are likely to be dinuclear in the solid state but form mononuclear species in solution. The complexes have an antiproliferative effect against both leukemia cell lines; complex **(2)** exhibits higher activity than cisplatin against U937 (8.20 *vs* 16.25 μmol dm^{-3}) and a comparable one against THP-1. These human neoplastic cells are also more susceptible than peripheral blood mononuclear cells (PBMCs) toward the tested compounds. Using C57BL/6 mice an LD_{50} of 55 mg kg^{-1} was determined for complex **(2)**, suggesting that this compound is almost four times less toxic than cisplatin (LD_{50}= 14.5 mg kg^{-1}). The mechanism of cell death promoted by ligand H2L2 and by complexes **(2)** and **(4)** was investigated by a range of techniques demonstrating that the apoptosis signal triggered at least by complex **(2)** starts from an extrinsic pathway involving the activation of caspases 4 and 8. This signal is amplified by mitochondria with the concomitant release of cytochrome c and the activation of caspase 9.

Keywords: copper(II) complexes; X-ray diffraction studies; apoptosis; THP-1, U937 and PBMC cells; Caspases; mechanism of cell death.

1. Introduction

Leukemia is a broad term covering a spectrum of diseases. It is part of a group of diseases affecting the blood, bone marrow and lymphoid system, and which are all known as hematological neoplasms. An estimated combined total of 156,420 people in the US were diagnosed with leukemia, lymphoma or myeloma in 2014. New cases of leukemia, lymphoma and myeloma accounted for 9 percent of the estimated 1,665,540 new cancer cases diagnosed in the US in 2014.[1] About 90% of all leukemia cases are diagnosed in adults. While the treatment of childhood leukemia has improved significantly (with an average 85-95% complete response (CR) rate and 80-90% long–term survival), the prognoses for adult leukemic patients are still unsatisfactory; the average CR rate is 70-80% but long-term survival is only 20-30%.[2-4]

The development of Gleevec® (imatinib mesylate, a tyrosine kinase inhibitor), frequently referred to as the "leukemia pill", has revolutionized CML (cronic myelogeneous leukemia) treatment. This oral drug was approved by the FDA for use in 2001.[5] In 2011, Sprycel (dasatinib, another tyrosine kinase inhibitor) was developed to treat CML, a drug that induces hematologic and cytogenic responses in patients who cannot tolerate or are resistant to imatinib mesylate. Its major side effect is reversible myelosuppression, and it was thus suggested that a successful long-term treatment of CML may require a cocktail of kinase inhibitors.[6]

Due to its biological relevance and the role copper plays in tumor angiogenesis,[7] especially in the early stage, a large number of copper(II) complexes have been synthesized and screened for anticancer activity; many of these derivatives display prominent *in vitro* cytotoxic activity.[8-10] However, very few *in vitro* studies on copper(II) complexes have been translated into preclinical *in vivo* models.[11-15] In 2014, Xu and co-workers reported anti-tumor activity of a copper complex containing disulfiram in its structure. This complex targets lymphoid malignant cell lines (Raji and Molt4 cells), *in vitro* and *in vivo*.[16] In 2015, Erxleben and co-workers reported results for a dinuclear copper(II)

complex, containing the ligand 2,6-bis(1,4,7-triazacyclonon- 1-ylmethyl)-4-methylphenol), which displays low toxicity against a human non-tumor cell line and IC_{50} values comparable or even lower than those of cisplatin against various cancer cell lines. Their complex interacts with DNA and activates the p53-dependent pathway of apoptosis.[17] Zhu and co-workers reported potent antitumoral activity against human cell lines (A549, Eca109 and SGC7901) for three mononuclear complexes containing the ligand H_2TBHP (2-(3,5-di-tert-butyl-2- hydroxybenzylamino)-2-benzyl-acetic acid). The associated apoptosis is related to the effect of these copper(II) complexes on the expression of p53, Bax and Bcl-2.[18]

In an earlier study we reported that the complex [Cu(HPClNOL)Cl]Cl. MeOH (HPClNOL= [1-(bis-pyridin-2-ylmethyl-amino)-3-chloropropan-2-ol) was able to promote DNA cleavage *in vitro* and was toxic to the THP-1 cell line, inducing cell death by apoptosis.[19] In a subsequent study we reported that the cytotoxic activity of the iron(III) complex [Cl(HPClNOL)Fe(III)(μ-O)Fe(III)(HPClNOL)Cl]Cl_2.2H_2O, employing the same HPClNOL ligand, takes place in the mitochondria, also involving so-called death receptors, which suggested that both pathways (intrinsic and extrinsic) may be involved in the apoptotic stimuli.[20] Attempting to search for more active compounds as well as to expand on our understanding of the events occurring within cells that were exposed to a cytotoxic agent, we have synthesized a family of new ligands (Scheme 1) and their copper complexes (Scheme 2).

HL1-H2L4 (see Scheme 1) are derived from the ligands HPClNOL and H_2BPClNOL (= 1-(bis-pyridin-2-ylmethyl-amino)-3-chloropropan-2-ol), which have previously led to the synthesis of compounds with interesting biological properties (*e.g.* antitumoral, antibacterial and antioxidant).[19-23] The main difference between those previously reported ligands (HPClNOL and H_2BPClNOL) and HL1-H2L4, is the presence of a naphthyl group in the latter. This modification was based on the demonstrated relevance of naphthalene derivatives as valuable pharmacologic compounds possessing

various important biological properties such as anti-inflammatory, antibacterial, hypotensive, bradycardiac and antitumoral activities.[24,25] Ligands HL1 and HL3 are isomers (possessing two pyridinic groups), as are H2L2 and H2L4 (possessing one phenolic and one pyridinic group). The biological activity of the corresponding copper complexes was assessed both *in vitro* and *in vivo* through the evaluation of IC_{50} (on human leukemia cell lines normal cells) and DL_{50} (mice) values. The interaction of the copper complexes with cancer cells was monitored *via* fluorescence and electron microscopies, cell cycle analysis, annexin staining, mitochondrial membrane potential ($\Delta\Psi m$) analysis, release of cytocrome *c* and the activation of caspases.

2. Experimental

2.1. Materials.

The ligands and their respective copper complexes were synthesized using analytical grade reagents. UV-Vis, electrochemical and MS investigations were carried out employing spectroscopic, HPLC or MS quality solvents. All chemicals and reagents were purchased from Aldrich (Sigma-Aldrich) and used as such.

2.2. Spectroscopic Measurements.

^{1}H and ^{13}C NMR spectra were recorded on a JEOL eclipse 400+ spectrometer. Chemical shifts (δ) are given in ppm, and the spectra were recorded in appropriate, deuterated solvents, as indicated. TMS (0 ppm) was employed as standard. Infrared spectra were recorded on a Shimadzu FT-IR 8300 spectrophotometer. The solid sample was prepared in a KBr pellet and spectra were recorded over the frequency range of 400-4000 cm^{-1}. UV-Vis spectra for all the ligands and copper complexes were recorded in methanol on a UV-Vis Varian, Cary 50 Bio. Full scan mass spectra (MS mode) were obtained on a MicroTOF LC Bruker Daltonics spectrometer equipped with an electrospray source

operating in positive ion mode. Samples were dissolved in a MeOH/H_2O (50/50) solution and were injected in the apparatus by direct infusion. EPR spectra were obtained using a Bruker E500 spectrometer with a high sensitive cylindrical cavity, operating at X-band (9 GHz) at 100 K. The following experimental settings were used: central magnetic field 3,200 G; sweep width 2,000 G; microwave power 2 mW; modulation frequency 100 kHz; modulation amplitude 10 G; receiver gain 60 dB; sweep time 180 s; time constant 20.48 ms; number of scans 1. The Qpow program[26] was used to simulate EPR spectra. Calibration of g-values was based on the g = 1.9797 signal of a MgO:Cr^{3+} marker.

2.3. X-ray crystallography.

A blue plate-like crystal with dimensions of 0.08 x 0.18 x 0.33 mm^3 was selected from a crystalline sample of complex **(2)** for crystallographic analysis. X-ray diffraction data were measured on a Kappa APEXII Duo diffractometer. Intensities were collected with ω and ϕ scans and were corrected for Lorentz and polarization effects. An empirical absorption correction (multi-scan) was also applied to all measured intensities with maximum and minimum transmission factors of 0.925 and 0.737, respectively. [27]A green plate-like crystal with dimensions of 0.11 × 0.23 × 0.28.mm^3 was selected from a crystalline sample of complex **(4)** for crystallographic analysis. X-ray diffraction data were measured on a Bruker D8 Venture diffractometer System with CMOS Photon 100 detector. Intensities were collected with ω and ϕ scans and were corrected for Lorentz and polarization effects. An empirical absorption correction (multi-scan) was also applied to all measured intensities with maximum and minimum transmission factors of 0.925 and 0.737, respectively. An empirical absorption correction (multi-scan) was also applied to all measured intensities with maximum and minimum transmission factors of 0.925 and 0.737, respectively. The structures were solved by direct methods and refined by full-matrix least-squares on F^2 using Shelx package.[28] The structures were solved by direct methods and

refined by full-matrix least-squares on F^2. All non-hydrogen atoms were refined with anisotropic displacement parameters. Hydrogen atoms bonded to C atoms were placed at their idealized positions using standard geometric criteria. H atoms of the coordinated alcohol group were located from Fourier difference maps. To complex (**2**), the contribution to the scattering of highly disordered molecules of solvate (probably water or methanol) was removed from the refinement using the squeeze procedure in the PLATON software.[29] The formula weight and density were calculated from the atom list. Potential solvent accessible voids of 244 $Å^3$ are observed in the crystal structure, which would contain 72 electrons per unit cell.Potential solvent accessible voids of 244 $Å^3$ are observed in the crystal structure. Further crystallographic information is presented in Table 1.

Table 1. Crystal data and structure refinement for complex **(2)** and **(4)**.

Compound	Complex (**2**)	Complex (**4**)
Empirical formula	$Cu_2C_{52}H_{52}Cl_2N_4O_6$, 2(Cl)	$Cu_2C_{52}H_{52}Cl_2N_4O_6$, 2(Cl), 4($CH_4O$)
Formula weight	1097.86	1226.04
Temperature (K)	190(2)	295(2)
Wavelength (Å)	0.71073	0.71073
Crystal system	Triclinic	Monoclinic
Space group	P-1	$P2_1/n$
Unit cell dimensions	a = 8.7095(2) Å b = 10.7960(3) Å c = 15.7740(3) Å; α= 86.9340(10)°. β= 77.2440(10)°. γ = 79.0790(10)°	a = 10.6604(13) Å b = 20.745(2) Å c = 13.384(2) Å; β= 97.439(6)º
Volume ($Å^3$)	1420.28(6)	2935.1(6)
Z	1	2
Density (calculated) (mg/m^3)	1.284	1.387
Absorption coefficient (mm^{-1})	0.984	0.965
F(000)	566	1276.0

Theta range for data collection (degree)	1.92 to 31.48	2.2 to 25.4
Index ranges	$-12 \le h \le 12$, $-15 \le k \le 15$, $-23 \le l \le 23$	$-11 \le h \le 12$, $-24 \le k \le 24$, $-16 \le l \le 15$
Reflections collected	32822	14227
Independent reflections	9416	5334
Observed reflections	7540	3967
R_{int}	0.0269	0.0331
Restraints	0	0
Parameters	312	348
Goodness-of-fit on F^2	1.068	1.033
Final R indices [$I>2\sigma(I)$]	R1 = 0.0385, wR2 = 0.1053	$R_1 = 0.0372$, $wR_2 = 0.0838$
R indices (all data)	R1 = 0.0503, wR2 = 0.1100	$R_1 = 0.0626$, $wR_2 = 0.0961$
Largest diff. peak and hole (e.$Å^{-3}$)	1.337 and -1.012	0.52 and -0.31

2.4. Conductivity Measurements and Melting Point Determination.

The electrical conductivity of a $1x10^{-3}$ mol dm^{-3} solution of each complex was measured with a Biocristal conductometer. Melting points were measured on a Microquimica MQAPF-301 apparatus.

2.5. Elemental Analyses.

The purity of tested compounds was determined by combustion elemental analyses conducted with a Thermo Scientific FLASH 2000 CHNS/O analyzer.

2.6. Cyclic Voltammetry Analyses.

Cyclic voltammograms (CVs) were carried out with an Autolab PGSTAT 10 potentiostat/galvanostat in acetonitrile containing 0.1 mol dm^{-3} tetrabutylammonium perchlorate ($TBAClO_4$) as the supporting electrolyte under argon atmosphere at room temperature. The electrochemical cell employed was a standard three-electrode configuration: a glassy carbon working electrode, a platinum-wire auxiliary electrode and a commercial Ag/AgCl electrode immersed in a salt bridge containing 0.1 mol dm^{-3} $TBAClO_4$. The formal potential of the ferrocenium/ferrocene couple

was 0.426 V *vs* the reference electrode Ag/AgCl, being established as 0.400 V *vs* NHE.[30]

2.7. Potentiometric Titration.

The potentiometric studies were carried out with a Corning 350 digital pH meter fitted with a blue-glass and Ag/AgCl reference electrodes calibrated to read -log[H^+] directly, designated as pH. Bidistilled water in the presence of $KMnO_4$ was used to prepare the solutions. The electrode was calibrated using the data obtained from the potentiometric titration of a known volume of a standard 0.100 mol dm^{-3} HCl solution with a standard 0.100 mol dm^{-3} KOH solution. The ionic strength of the HCl solution was maintained at 0.100 mol dm^{-3} by addition of KCl. The measurements were carried out in a thermostated cell containing the compound or ligand solution (0.5 mmol/50 cm^3) with ionic strength adjusted to 0.100 mol dm^{-3} by addition of KCl, at 25.00ºC. The experiments were performed under argon flow to eliminate the presence of CO_2. The samples were titrated by addition of fixed volumes of a standard CO_2-free KOH solution (0.100 mol dm^{-3}). Computations were carried out with the BEST7 program, and species distribution diagrams were obtained with SPE and SPEPLOT programs.

2.8. Syntheses of Ligands.

2.8.1.Synthesis of HL1.

Ligand HL1 (Scheme 1) was prepared by the reaction between bis-(pyridin-2-ylmethyl)amine[31] (0.025 mol, 4.98g) and 2-(1-naphthylmethyl)oxirane (0.025 mol, 5g), in ethanol. The mixture was stirred for 5 days at room temperature, which was follow by TLC, using ethanol as eluent. Subsequently, the solvent was removed under reduced pressure and the residue was to 50 cm^3 of water. The compound was extracted with five 50 cm^3 portion of $CHCl_3$ and the extracts were combined, washed with brine, dried over anhydrous $MgSO_4$, filtered and concentrated under reduced pressure. A

brown oil was obtained. Yield: 6.5g (65%).^{1}H NMR (400 MHz, $CDCl_3$) δ/ppm: 2.96 (dd, 1H), 3.12 (dd, 1H), 3.97 (d, 2H), 4.05-4.09 (m, 3H), 4.19 (dd, 1H), 4.28- 4.35 (m, 1H), 6.77 (d, 1H), 7.12-7.16 (m, 4H), 7.32-7.36 (m. 1H), 7.39 (dd, 1H), 7.46 (t, 2H), 7.58 (t, 2H), 7.76 (d, 1H), 8.09 (d, 1H), 8.56 (m, 2H). ^{13}C NMR (100 MHz, $CDCl_3$) δ/ppm: 58.20, 60.78 (2C), 67.99, 70.27, 104.87, 120.50, 122.26, 122.42 (2C), 123.43 (2C), 125.26, 125.78, 126.07, 126.29, 127.59, 134.64, 136.88 (2C), 149.21 (2C), 154.65, 157.28(2C).IR (cm-1) ν: 3700-3100, 3051, 2928, 2839, 1628, 1589, 1508, 1435, 1269, 791, 771.UV-Vis λ(nm) data (ε, dm^3 mol^{-1} cm^{-1}): 210 ($7.39x10^4$), 230 ($4.79x10^4$), 262 ($1.29x10^4$), 267 ($1.24x10^4$), 292 ($9.64x10^3$), 305 ($6.35x10^3$), 320 ($3.7x10^3$).

2.8.2. Synthesis of H2L2.

The Ligand H2L2 (See Scheme 1) was prepared employing a similar method, but using 2-(hydroxybenzyl)(2-pyridylmethyl)amine)[32] (0.025 mol, 5.35g) in place of bis-(pyridin-2-ylmethyl)amine. The mixture was stirred at room temperature and after one day a white solid was obtained, which was removed by filtration. The solid was recrystallized in hot hexane. After standing the solution for a few days a crystalline white solid was filtered off and dried with ether. Yield: 6.6g (64%).m.p. 140ºC. Anal. Calcd for $C_{26}H_{26}N_2O_3$; MW = 414.5 g mol^{-1} : C, 75.34; H, 6.32; N, 6.76. Found: C, 75.65; H, 6.59; N, 6.64%. ^{1}H NMR (400 MHz, $CDCl_3$) δ/ppm: 3.00 (dd, 2H), 3.79-3.84(m, 1H), 3.91-4.00 (m, 1H), 4.03-4.08 (m, 2H), 4.13 (d, 1H), 4.15-4.19 (m, 1H), 4.35-4.39 (m, 1H), 6.77 (d, 1H), 6.81 (t, 1H), 6.89 (d, 1H), 7.06 (d, 1 H), 7.17-7.25 (m, 3H), 7.34 (t, 1H), 7.41-7.44 (m, 1H), 7.48 (t, 2H), 7.69 (t, 1H), 7.78 (d, 1H), 8.03 (d, 1H), 8.63 (d, 1H).

^{13}C NMR (100 MHz, $CDCl_3$) δ/ppm: 56.90, 58.61, 58.72, 67.72, 70.09, 104.71, 116.67, 119.14, 120.43, 121.80, 122.32, 122.54, 123.26, 125.12, 125.43, 125.80, 126.29, 127.39, 129.21, 129.60, 134.39, 137.18, 148.81, 154.14, 157.28, 157.45. IR (cm-1) ν: 3300-2800, 2927, 2831, 1581, 1489, 1400, 1269, 1242, 791, 756. UV-Vis λ(nm) data (ε, dm^3 mol^{-1} cm^{-1}): 209 ($1.21x10^5$), 231 ($7.47x10^4$), 268

($1.89x10^4$), 280 ($1.99x10^4$), 293 ($1.64x10^4$), 306 ($1.11x10^4$), 319 ($6.8x10^3$).

2.8.3. Synthesis of HL3.

The same methodology employed for the synthesis of HL1 was employed here, but now using 2-(2-naphthylmethyl)oxirane (0.025 mol, 5g) (See Scheme 1). A brown oil was obtained. Yield: 7.1g (71%). ^{1}H NMR (400 MHz, $CDCl_3$) δ/ppm: 2.89 (m, 1H), 3.04 (dd, 1H), 3.92-4.12 (m, 6H), 4.21-4.26 (m, 1H), 7.11 (d, 4H), 7.26-7.31 (m, 3H), 7.40 (t, 2H), 7.68-7.74 (m, 2H), 7.56 (t, 2H), 8.54 (d, 2H). ^{13}C NMR (100 MHz, $CDCl_3$) δ/ppm: 58.41, 60.73 (2C), 67.94, 70.42, 106.88, 119.21, 122.42 (2C), 123.41, 123.82 (2C), 126.52, 127.00, 127.83, 129.19, 129.50, 134.71, 136.88 (2C), 149.18 (2C), 156.99, 159.25 (2C). IR (cm^{-1}) ν: 2800-3300, 3055, 2928, 2835, 1628, 1597, 1512, 1469, 1258, 837, 752, 771. UV-Vis λ(nm) data (ε, $dm^3\ mol^{-1}\ cm^{-1}$): 225 ($9.06x10^4$), 262 ($1.5x10^4$), 270 ($1.26x10^4$), 281 ($6.12x10^3$).

2.8.4. Synthesis of H2L4.

The ligand H2L4 (See Scheme 1) was prepared employing similar method described for H2L2. A brown-redish oil was obtained. Yield: 7.0g (67%). ^{1}H NMR (400 MHz, $CDCl_3$) δ/ppm: 2.91 (m, 2H), 3.78 (d, 1H), 3.92-4.00 (m, 2H), 4.02-4.04 (m, 1H), 4.25-4.28 (m, 1H), 6.79 (t, 1H), 6.87 (dd, 1H), 7.02-7.04 (m, 2H), 7.07-7.10 (m, 2H), 7.17 (d, 2H), 7.22 (t, 1H), 7.32 (t, 1H), 7.42 (t, 1H), 7.65 (dd, 1H), 7.68-7.71 (m, 1H), 7.74 (d, 1H), 8.61 (m, 1H). ^{13}C NMR (100 MHz, $CDCl_3$) δ/ppm: 57.09, 58.71, 58.99, 67.75, 70.34, 106.97, 116.67, 118.81, 119.27, 122.50, 122.68, 123.37, 123.77, 126.42, 126.92, 127.69, 129.19, 129.26, 129.42, 129.74, 134.29, 137.37, 148.92, 156.58, 157.40, 157.57.

IR (cm^{-1}) ν: 3455, 3053, 2949, 2845, 1628, 1599, 1508, 1477, 1395, 1267, 1258, 839, 763, 748. UV-Vis λ(nm) data (ε, $dm^3\ mol^{-1}\ cm^{-1}$): 225 ($1.02x10^5$), 262 ($1.1x10^4$), 270 ($1.07x10^4$), 281 ($6.46x10^3$). See Scheme 1.

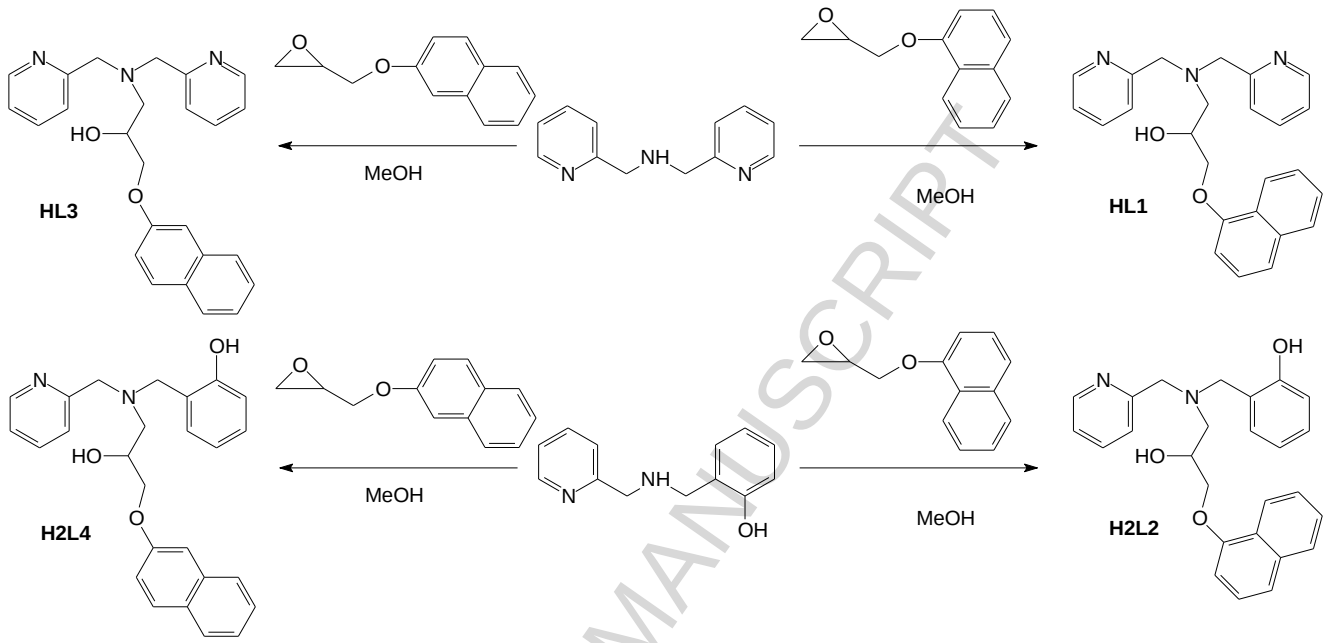

Scheme 1. Scheme of synthesis for ligands HL1-H2L4.

2.9. Syntheses of copper complexes.

2.9.1. Synthesis of [(HL1)Cu(μ-Cl)$_2$Cu(HL1)]Cl$_2$.H$_2$O (1).

Complex **(1)** (Scheme 2) was prepared in a reaction between HL1 (1.0 mmol, 0.398g) and $CuCl_2.6H_2O$ (1.0 mmol, 0.1705 g) in ethyl acetate, with constant stirring at room temperature. After allowing the blue solution to stand for a few days a microcrystalline blue solid was filtered off and dried with ether. Yield: 0.34g (62%). m.p. 197ºC. IR (cm^{-1}): ν(OH), 3425-3483 (s); ν(CH), 3047 and 3008 (s); ν(CH$_2$), 2936(s); ν(CH$_2$), 2881 (s); (C=C and C=N), 1609 (s), 1578 (s), 1443 (s) and 1396 (s); ν(C-O-C), 1269 (s); γ (CH), 798 (s) and 775 (s). Anal. Calcd for [(HL1)Cu(μ-Cl)$_2$Cu(HL1)]Cl$_2$. H$_2$O **(1)** ($C_{50}H_{52}Cu_2Cl_4N_6O_5$, MW= 1086 g mol^{-1}): C, 55.30; H, 4.83; N, 7.74. Found: C, 55.49; H, 4.64; N, 7.85%. UV-Vis λ(nm) data (ε, dm^3 mol^{-1} cm^{-1}): 209 (1.54x10^4), 230 (1.01x10^4), 262 (9.49x10^4), 267 (5.99x10^4), 292 (1.92x10^4), 305 (1.69x10^4), 320 (5.66x10^3), 707 (77.91). Ω= 83 μS cm^{-1} (1:1

electrolyte- MeOH). MS (ESI) in H_2O/MeOH 1:1: $[M]^+$ = 497: $[Cu(HL1)Cl]^+$. $E_{1/2}$= -0.324 V vs NHE (Cu^{II}/Cu^{I}).

*2.9.2. Synthesis of [(H2L2)Cu(μ-Cl)$_2$Cu(H2L2)]Cl$_2$.5H$_2$O **(2)**.*

Complex **(2) (**Scheme 2) was obtained using H2L2 (1.0 mmol, 0.414g) in place of HL1, using mixture of ethylacetate/methanol (3:2) as solvent. After allowing the green solution to stand for a few days a microcrystalline green solid was filtered off and dried with ether. Yield: 0.52g (90%). m.p. 150ºC. IR (cm^{-1})**:** ν(OH), 3348 (b); ν(CH), 3047 (s); ν(CH_2), 2931(s); ν(CH_2), 2712 (s); (C=C and C=N), 1613 (s), 1578 (s), 1447 (s) and 1400 (s); ν(C-O-C), 1269 (s); ν(C-O), 1242 (s); γ(CH), 798 (s) and 748 (s). Anal. Calcd for [(H2L2)Cu(μ-Cl)$_2$Cu(H2L2)]Cl$_2$.5H$_2$O **(2)** ($C_{52}H_{62}Cu_2Cl_4N_4O_{11}$, MW= 1187.91 g/mol): C, 53.38; H, 5.17; N, 4.79. Found: C, 53.22; H, 5.52; N, 4.77 %. UV-Vis λ(nm) data (ε, $dm^3\ mol^{-1}\ cm^{-1}$): 208 ($6.09x10^4$), 230 ($3.73x10^4$), 268 ($9.37x10^4$), 288 ($1.11x10^4$), 306 ($6.29x10^3$), 320 ($3.19x10^3$), 444 (18.21), 722 (72.07). Ω= 111 μS cm^{-1} (1:1 electrolyte- MeOH). MS (ESI): $[M]^+$ = 512 $[Cu(H2L2)Cl]^+$. E_{pa}= 0.164 and E_{pc}= -0.588 V vs NHE. The respective complex could be obtained as single crystals suitable for x-ray diffraction when ethanol is employed in place of ethylacetate/methanol, under heating for 10 h. Anal. Calcd for [(H2L2)Cu(μ-Cl)$_2$Cu(H2L2)]Cl$_2$ **(2)** $C_{52}H_{52}Cu_2Cl_4N_4O_6$, MW= 1097 g mol^{-1}): C, 52.57; H, 5.26; N, 4.72. Found: C, 52.73; H, 5.39; N, 4.94%. m.p. 150ºC. Ω= 111 μS cm^{-1} (1:1 electrolyte- MeOH).

2.9.3.Synthesis of [(HL3)Cu(μ-Cl)$_2$Cu(HL3)]Cl$_2$.4H$_2$O **(3)**.

Complex **(3) (**Scheme 2) was obtained using ethyl acetate and HL3 (1.0 mmol, 0.398g) in place of HL1. After allowing the green solution to stand for a few days a microcrystalline dark green solid was filtered off and dried with ether. Yield: 0.25g (45%). m.p. 136ºC. IR (cm^{-1}): ν(OH), 2750-3605 (b); ν(CH), 3103, 3057 and 3021 (s); ν(CH_2), 2951(s); 2932(s) 2878 (s); (C=C and C=N), 1627 (s),

1609(s), 1508 (s), 1468 (s) and 1442 (s); ν(C-O-C), 1259 (s); γ (CH), 834 (s) and 769 (s). Anal. Calcd for $[(HL3)Cu(\mu\text{-}Cl)_2Cu(HL3)]Cl_2.4H_2O$ **(3)** $C_{50}H_{58}Cu_2Cl_4N_6O_8$, MW= 1140 g mol^{-1}): C, 52.68; H, 5.13; N, 7.37. Found: C, 52.51; H, 5.58; N, 7.54%. UV-Vis λ(nm) data (ε, dm^3 mol^{-1} cm^{-1}): 225 ($9.74x10^4$), 259 ($1.72x10^4$), 270 ($1.23x10^4$), 281 ($7.16x10^3$), 702 (68.69). Ω= 82 μS cm^{-1}(1:1 electrolyte- MeOH). MS (ESI): $[M]^+$ = 497 $[Cu(HL3)Cl]^+$. $E_{1/2}$= -0.348 V vs NHE (Cu^{II}/Cu^{I}).

*2.9.4.Synthesis of $[(H2L4)Cu(\mu\text{-}Cl)_2Cu(H2L4)]Cl_2.6H_2O$ **(4)**.*

Complex **(4)** (Scheme 2) was obtained using H2L4 (1.0 mmol, 0.414g) in place of HL1, using an ethyl acetate/methanol mixture (3:2). After allowing the green solution to stand for a few days a microcrystalline green solid was filtered off and dried with ether. Yield: 0.58g (97%). m.p. 105ºC. IR(cm^{-1}): ν(OH), 3350-3000 (b); ν(CH), 3059 (s); $\nu(CH_2)$, 2931(s); $\nu(CH_2)$, 2873 (s); (C=C and C=N), 1628 (s), 1597 (s), 1508 (s), 1458 (s) and 1399 (s); ν(C-O-C), 1257 (s); ν(C-O), 1247 (s); γ(CH), 844 (s) and 760 (s). Anal. Calcd for $[(H2L4)Cu(\mu\text{-}Cl)_2Cu(H2L4)]Cl_2.6H_2O$ **(4)** ($C_{52}H_{64}Cu_2Cl_4N_4O_{12}$, MW= 1206 g mol^{-1}): C, 51.79; H, 5.35; N, 4.65. Found: C, 51.96; H, 5.66; N, 4.70%. UV-Vis λ(nm) data (ε, dm^3 mol^{-1} cm^{-1}): 225.94 ($9.68x10^3$), 262.22 ($1.4x10^3$), 270.04 ($1.34x10^3$), 281.97 ($1.07x10^3$), 440.32 (29.58), 731.93 (68.34). Ω= 108 μS cm^{-1} (1:1 electrolyte, MeOH). MS (ESI): $[M]^+$= 512 $[Cu(H2L4)Cl]^+$. E_{pa}= 0.10 and E_{pc}= -0.548 V vs NHE. The respective complex could be obtained as single crystals suitable for x-ray diffraction when methanol is employed in place of ethylacetate/methanol, under heating for 10 h, resulting in the complex $[(H2L4)Cu(\mu\text{-}Cl)_2Cu(H2L4)]Cl_2.4CH_3OH$.

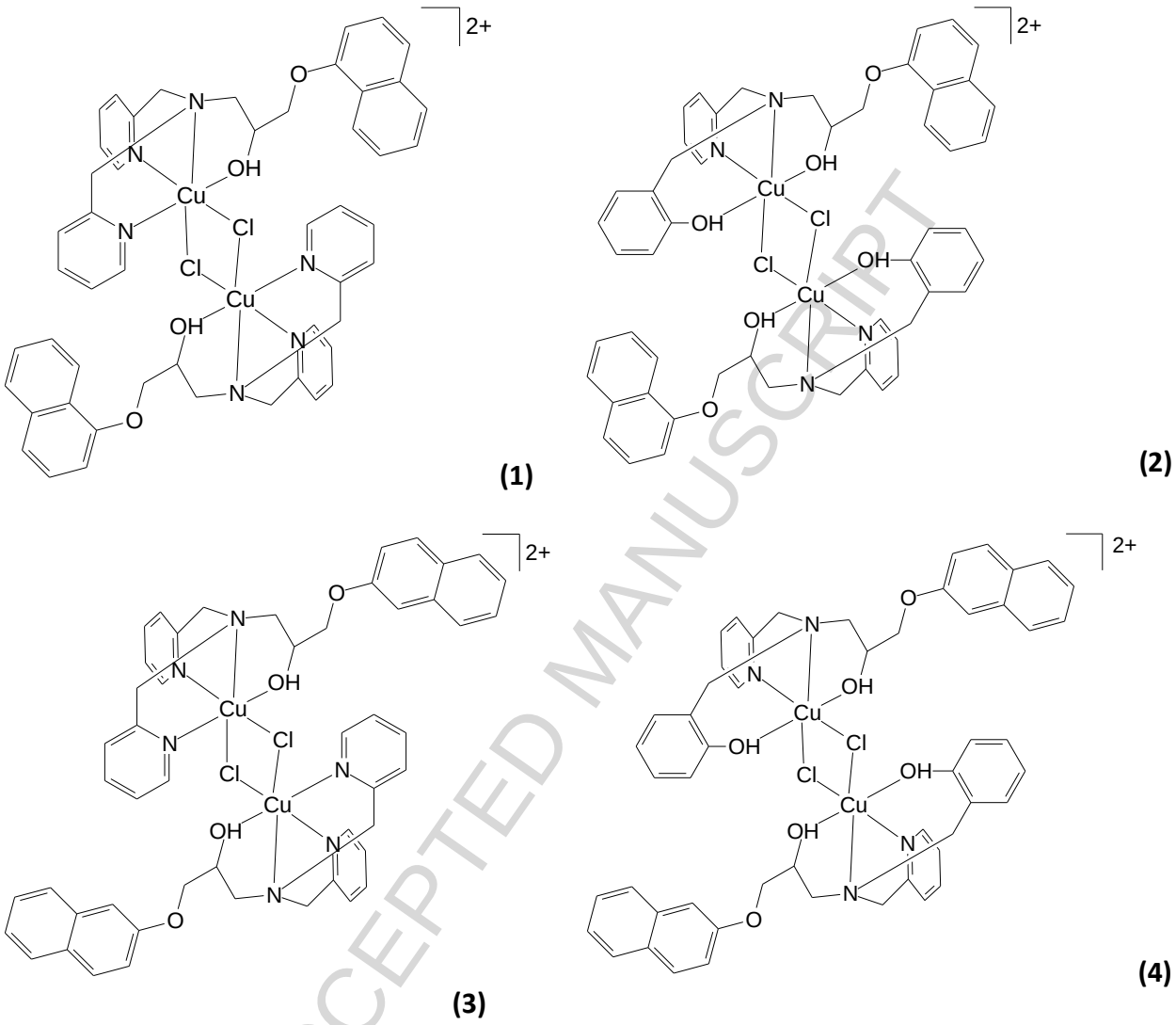

Scheme 2. Structures of complexes **(1)-(4)**. The proposed structures are based on X-ray diffraction data performed for complexes **(2)** and **(4)**.

2.10. Culture of leukemia cell lines.

Human leukemia cell lines THP-1 (acute monocytic leukemia cell line) and U937 (histiocytic lymphoma cell line) were cultured routinely in DMEM-F12 medium (Gibco, BRL), supplemented with 10% fetal calf serum and gentamicyn (20mg/ml, Gibco, BRL) at 37 °C in a humidified atmosphere containing 5% CO_2 in air. Culture media were changed every 2–3 days.

2.11. Isolation of normal human peripheral blood mononuclear cells (PBMC).

Blood samples were collected from health donors in Sodium Heparin glass tubes "VacutainerTM" (Becton Dikinson) and the PBMC were isolated over Ficoll-Paque™ Plus (1.08g cm^{-3}) in a 50 cm^3 conical tube (2:1 - blood:ficoll). Twenty milliliters of a fresh, heparinized blood sample was diluted in phosphate buffer saline (PBS), gently laid over 10 cm^3 of Ficoll and centrifuged at 500xg for 20 min at 25 °C. PBMC were collected from the interface of spun blood samples and were washed three times with PBS by centrifugation at 500xg for 10 min at 4 °C. The supernatant was discarded and the cells were suspended in DMEM-F12 medium (Gibco, BRL). A 0.4% Trypan blue solution (Sigma, Germany) was used to dissolve the cells into an appropriate concentration and the viability of cells was checked; the required range of cells' viability is 95-99%.

2.12. Analysis of cell viability by MTT assay.

Cells (U937, THP-1 and PBMC) were plated (approximately 1 x 10^6 cells) in 96-well plates and treated with different concentrations of ligands and their respective copper complexes for 36 h in DMEM-F12 medium (Gibco, BRL). Cell viability was measured by the colorimetric microassay (MTT assay). Twenty microliters of 3-(4,5-dimethyl- 2-thihazyl)-2,5-diphenyl-2H-tetrazolium bromide (MTT) stock solution (5 mg cm^{-3}) were added into each well, and the cells were incubated at 37 °C for 4 hour. Then, the MTT-formazan produced by viable cells was dissolved in an isopropanol-HCl solution. The optical density (OD) values were measured by spectrophotometry at 570 nm using a Microplate Reader (Epoch™, BioTek® Instruments, Inc.). The OD values are presented as relative viable cell numbers, which were expressed in percentages (%). Relative cell viability = OD of treated sample/Mean OD of control sample.

2.13. Determination of in vivo acute toxicity for complex **(2)**.

In order to determine the *in vivo* acute toxicity of complex **(2)**, male and female C57BL/6 mice, between 18 g and 25 g were separated into groups of 4 animals. The complex was injected into the peritoneal cavity, such that each group received the respective concentrations of the compound (25, 50, 100, 200 mg kg^{-1}). For inoculation we used a 3 cm^3 syringe and a hypodermic sterile needle SR 0.45 mm x 13 mm NIPRO. The vehicle used for administration of the complex was ultrapure water. The animals were observed closely for at least 4 hours post-injection and in 24 h intervals for 30 days thereafter. After this period, median lethal dose (LD_{50}), a dose required to kill half the members of a tested population, was determined. The research protocol was approved by the Ethical Committee for Animal Experimentation of Universidade Estadual do Norte Fluminense Darcy Ribeiro, under protocol number 214/2014.

2.14. Analysis of apoptosis and necrosis cell death by fluorescence microscopy.

Cells (~1 x 10^6) were plated in 96-well plates and treated with ligand H2L2 (80 and 160 μmol dm^{-3}) and complexes **(2)** (40 and 80 μM) and **(4)** (80 and 160 μM) for 12, 24 and 36 h in DMEM-F12 medium (Gibco, BRL). Then, the acridine orange/ethidium bromide double staining was used to identify the following four cell stages according to Kosmider et al.:[33] 1) living cells (green nucleus with red–orange cytoplasm), 2) early apoptosis (cell membrane still continuous but chromatin condensation and an irregular green nucleus are visible), 3) late apoptosis (so-called ‘secondary necrosis’ or ‘apoptotic necrosis’: ethidium bromide penetrates through altered cell membrane and stains the nuclei orange, while fragmentation or condensation of chromatin is still observed), 4) necrosis (uniformly orange-stained cell nuclei). Following the addition of fluorochromes (25 μg cm^{-3} acridine orange and 50 μg cm^3 ethidium bromide), 300 cells were immediately analyzed in each of two independent experiments using fluorescence microscopy (Axioplan – Carl Zeiss microscope).

2.15. Measurement of annexin V and propidium iodide staining.

U937 and THP-1 (1 x 10^6 cells cm^{-3}) were cultured in 24-well plates and treated with 50 and 100 μmol dm^{-3} of complex **(2)** for 12 h. Apoptosis was detected by using the Annexin V-FITC Apoptosis Detection Kit (SIGMA-ALDRICH). Briefly, after incubation cells were washed twice with phosphate buffered saline (PBS), and incubated in 0.5 cm^3 of binding buffer (100 mmol dm^{-3} HEPES/NaOH, pH 7.5, 1.4 mol dm^{-3} NaCl and 25 mmol dm^{-3} $CaCl_2$). To each sample was added 5 mm^3 of Annexin V-FITC and 10 mm^3 of PI. Samples were incubated at room temperature for 10 min, protected from light. Cell fluorescence was determined immediately with a flow cytometer (FACS Calibur-BD Sciences). Each experiment per sample was determined by recording 10,000 events.

2.16. Detection of apoptosis by DNA fragmentation and agarose gel electrophoresis.

U937 and THP-1 cells (1 x 10^6 cells cm^3) were plated in 6 multiwell plates and treated with 50 and 100 μmol dm^{-3} of complex **(2)** for 12h. After incubation, cells were harvested, transferred to microtubes, washed twice with PBS and fixed in 70% ethanol at -20 ºC for 2 h. After centrifugation ethanol was totally removed, dried and evaporated at room temperature. The cells were resuspended in 50 mm^3 of extraction buffer (0.2 mol dm^{-3} Na_2HPO_4 and 0.1 mol dm^{-3}, pH 7.8) and incubated at 37°C for 30 min. 5 mm^3 RNAse (1mg cm^3) was added in each sample and a new incubation was done at 3 °C for 30 min. 5 mm^3 of Proteinase K (1mg/mL) was added to each sample. To detect the DNA fragments, the isolated DNA samples were electrophoresed for 60 min at 60 V in a 1% agarose gel and stained with GelRed Nucleic Acid Stain (Biotium). DNA fragmentation was observed in a UV transilluminator (Bio-Rad, Gel Doc™ XR+).

2.17. Study of cell cycle arrest by flow cytometric analysis.

Cells (1 x 10^6) were plated in 24-well plates and treated with ligands H2L2 and H2L4 (80 μmol

dm^{-3}) and complexes **(2)** (40 μmol dm^{-3}) and **(4)** (80 μmol dm^{-3}) for 36h in DMEM-F12 medium (Gibco, BRL). After incubation the cells were fixed in 70% ethanol at 4 ºC for 30 min and stained with propidium iodide (PI) for 2 h in darkness. The DNA content was measured with a flow cytometer (FACS Calibur-BD Sciences) and cell cycle distribution was analyzed by WinMDI version 2.9 software.[34] The proportions of cells in the G_0/G_1, S, and G_2/M phases were represented as DNA histograms. Apoptotic cells with hypodiploid DNA content were measured by quantifying the sub-G_1 peak in the cell cycle pattern. Each experiment per sample was determined by recording 10,000 events.

2.18. Analysis of the mitochondrial membrane potential (ΔΨm) by flow cytometry using JC-1 stain.

U937 and THP-1 cells (1 x 10^6) were seeded in 24-well plates and treated with ligands H2L2 and H2L4 (80 μmol dm^{-3}) and complexes **(2)** (40 μmol dm^{-3}) and **(4)** (80 μmol dm^{-3}) for 36 h in DMEM-F12 medium (Gibco, BRL). Subsequently, the cell suspension was transferred to a sterile tube and pelleted (400xg for 7 min at room temperature). Cells were stained with the JC-1 dye (25μg cm^3) and incubated at 37 °C in a 5% CO_2 incubator for 15 minutes. The cells were washed twice with fresh medium and analyzed immediately by flow cytometry. JC-1 (5,5',6,6'-tetrachloro 1,1',3,3' tetraethylbenzimidazolylcarbocyanine iodide) exists as a monomer in the cytosol (green) but accumulates as red aggregates in the mitochondria. Generally, in apoptotic and necrotic cells, JC-1 exists in monomeric green form. Thus, mitochondria containing red JC-1 aggregates represent healthy cells that are detectable in the FL2 channel and express intact (ΔΨm), whereas green JC-1 monomers in apoptotic cells are detectable in the FITC channel (FL1) and express the loss of (ΔΨm). The mitochondrial transmembrane potential (ΔΨm) was measured with a flow cytometer (FACS Calibur) and analyzed by WinMDI version 2.9 software.[34]

2.19. Subcellular fractionation and detection of cytochrome C release.

U937 cells were plated at a 1 x 10^6 concentration in 24-well plates and treated with 40 µM of complex **(2)** for 6, 12, 24 and 36 h in DMEM-F12 medium (Gibco, BRL), supplemented with 10% fetal calf serum and 20 µg cm^{-3} gentamicin (Gibco, BRL). The mitochondrial fraction (MF) was separated from the cytoplasmic fraction (CF) using a digitonin-based subcellular fractionation technique to quantify the cytochrome c released in both fractions. Briefly, U937 cells were harvested by centrifugation at 800xg, washed in PBS, pH 7.2, and re-pelletted. Cells were then digitonin-permeabilized for 5 min on ice at a density of 3x 10^6 cells cm^{-3} in cytosolic extraction buffer (250 mmol dm^{-3} sucrose, 70 mmol dm^{-3} KCl, 137 mmol dm^{-3}, NaCl, 4.3 mmol dm^{-3} Na_2HPO_4, 1.4 mmol dm^{-3} KH_2PO_4 pH 7.2, 10 mg cm^{-3} leupeptin, 2 mg cm^{-3} aprotinin, containing 200 mg cm^{-3} digitonin). Plasma membrane permeabilization of cells was confirmed by staining in a 0.2% trypan blue solution. Cells were then centrifuged at 1000xg for 5 min at 4 °C. The supernatants (cytosolic fractions) were saved and the pellets solubilized in the same volume of mitochondrial lysis buffer (50 mmol dm^{-3} TRIS, pH 7.4, 150 mmol dm^{-3} NaCl, 2 mmol dm^{-3} EDTA, 2 mmol dm^{-3} EGTA, 0.2 % Triton X-100, 0.3% NP-40, 10 mg cm^{-3} leupeptin, 2 mg cm^{-3} aprotinin), followed by pelletting at 10,000xg for 10 min at 4 °C. Cytochrome c was quantified according to the protocol in the Cytochrome c ELISA KIT (Calbiochem®). The optical density (OD) values were measured by spectrophotometry at 450 nm using a Microplate Reader (Epoch™, BioTek® Instruments, Inc.).

2.20. Determination of caspase activities.

Caspases 3, 8 and 9 activities were determined using the substrates VDVAD-pNA or DEVD-pNA (caspase 3 substrates), IETD-pNA (a caspase 8 substrate), and LEHD-pNA (a caspase 9 substrate) following the protocols of the Caspase Activity Assay kit from Invitrogen™ (ApoTarget™ caspase

colorimetric protease assay kit). U937 cells (3-5 x 10^6/mL) were incubated with 40 μmol dm^{-3} of complex **(2)** for 3, 6 and 12 h and centrifuged at 400g for 10 min. The supernatant was removed, and the pellet was suspended in 0.1 cm^3 of lysis buffer and incubated on ice for 10 min followed by centrifugation at 10.000g for 1min. Protein concentrations were determined and cytosol extracts were diluted to a concentration of 50-200 μg protein per 50 mm^3 cell lysis buffer (1-4mg cm^3). Aliquots (50 mm^3) of the supernatant were removed and placed in a 96-well microplate containing reaction buffer (Invitrogen™). 5 mm^3 of each substrate was added, and the microplate was incubated at 37 °C for 12 h. Activity was monitored as the cleavage and release of free pNA and quantified at 405 nm using a Microplate spectrophotometer (Epoch™, BioTek® Instruments, Inc.). Caspase activation of treated cells was compared with an uninduced control sample for the determination of the fold increase in caspase activity.

2.21. Analysis of mitochondrial morphology by fluorescence imaging and transmission electron microscopy (TEM).

Fluorescence imaging of mitochondria: U937 cells were cultured at 1 x 10^6 cells cm^3 in 24-well plates and treated with 40 μmol dm^{-3} of complex **(2)** for 12 h. Cell suspensions were transferred to a sterile tube and pelleted (400xg for 5 min at room temperature). Then, cells were incubated with 100 nmol dm^{-3} Mitotracker CMXRos (Invitrogen, Molecular Probes) and 1 μg cm^3 Hoechst nuclear stain (Invitrogen, Molecular Probes) for 20 min, washed two times with PBS, resuspended in fresh D-MEM F12 medium and imaged using a fluorescence microscope (Axioplan – Carl Zeiss microscope). U937 cells (1x10^6 cells) were cultured in tissue culture bottles (25 cm^2) for 12 h. The cells were incubated with complex **(2)** (40 μmol dm^{-3}) for 12 h and centrifuged at 1200 rpm for 10 min and washed three times with phosphate-buffered saline (PBS; pH 7.2). The cell pellets were fixed for 1 h in 1% glutaraldehyde, 5 mM $CaCl_2$, 5% sucrose and 0.1 M cacodilate buffer. Fixed cells were washed three

times in a 5% sucrose solution in 0.1 M cacodilate buffer and post-fixed for 2 h protected from light in a 1:1 osmium/potassium ferrocianate solution. Post-fixed cells were washed twice with PBS and dehydrated sequentially in a graded series of acetone solutions (30, 50, 70, 90 and 100%). The cells were then soaked overnight in a 1:1 ratio of acetone and embedding resin (EPON®). The resin-embedded cells were placed in tubes and the tubes were placed at 37 °C in a humidified atmosphere for 48 h for polymerization of the resin. The polymerized blocks were sectioned and ultrathin sections were prepared. The effects of the complexes on U937 mitochondria were evaluated using a transmission electronic microscope (TEM-900, Zeiss, Germany).

2.22. Statistical Analysis.

For analysis of cell viability and apoptosis the mean and standard error were calculated from the raw data and then subjected to the One way ANOVA analysis (analysis of variance). A significant difference was taken as $p < 0.5$, <0.01 and <0.001.

3. Results and discussion

3.1. Syntheses and structures of copper(II) coordination compounds.

A group of similar ligands was developed in order to probe the influence of the chelating groups and structural isomerism introduced by them on their coordination behavior, as well as to gain insight into the influence of these features on the antitumor activity of their copper(II) complexes.

Ligands HL1 and HL3 present two pyridine groups, a tertiary amine and an alcohol function as chelating groups and an α-naphthyl or β-naphthyl group as pendant unit, respectively, providing a N3O coordination environment for the metal center. Ligands H2L2 and H2L4 are similar, presenting a pyridine, a phenol, a tertiary amine and an alcohol group, in addition to an α-naphthyl or β-naphthyl group, respectively, providing a N2O2 coordination environment for the metal center (Scheme 1). We

have previously published the synthesis of copper complexes containing ligands (HPClNOL[19] and H_2BPClNOL[23]) similar to those reported herein. The main difference is the lack of the naphthyl group in the earlier ligands. The relevance of the naphthyl units in the design of anticancer drugs has been assessed previously by Das and co-workers, which reported the cytotoxic activity of alkyl derivatives of 2-naphtol against four human cancer cell lines (Hep G2, A549, MDA 231 and HeLa). The IC_{50} values found for those compounds are comparable to that of doxorubicin.[25]

The four new ligands were characterized by IR and NMR. Their respective copper complexes are stable in air and are remarkably soluble in solvents such as DMF and DMSO, and slightly soluble in H_2O, CH_3CN, ethanol, methanol and chloroform. The reactions between these ligands and $CuCl_2.2H_2O$ allowed the isolation of monocrystals for complexes **(2)** and **(4)**, while compounds **(1)** and **(3)** were isolated as microcrystalline material. It was thus only possible to determine the molecular structure through X-ray diffraction for compounds **(2)** and **(4)**, but the structures for compounds **(1)** and **(3)** were modeled based on that of compounds **(2)** and **(4)**.

3.2. Description of Crystal Structures of Complexes (2) and (4).

The structure determination of complexes **(2)** and **(4)** reveals a center of symmetry situated in the plane formed by the Cu1-Cl1-Cu1´-Cl1´ atoms. The two monomeric units in the dimeric structure are symmetrically related. A perspective view of the cations is displayed in Figure 1, where the arrangements exhibited by the complexes are related to the inherent asymmetry of the ligands. The bond lengths and angles for complexes are listed in Table 2.

The coordination behavior of the ligands H2L2 and H2L4 is similar to that observed for the ligand H_2BPClNOL.[23] Interestingly, the X-ray diffraction study of the copper complex of this ligand revealed the presence of a mono- and a dinuclear species in the same unit cell. For H2L2 and H2L4 only the dinuclear species was observed, demonstrating that the large naphthyl group present in these

ligands does not exert an effect on the coordination mode of the ligands. The nitrogen atoms and the alcohol group present bond distances very similar to those observed for the compound $\{[Cu^{II}(H_2BPClNOL)]–\mu\text{-}(Cl)_2–[Cu^{II}(H_2BPClNOL)]\}Cl_2$. However, the Cu-$O_{phenol}$ is longer in **(2)** (2.5939(14) Å) and **(4)** (2.495(2) Å) than in the cited compound (2.446(2) Å), while the length of the Cu-Cl` bond is shorter in **(2)** and **(4)** (2.8657(4) and 2.8823(8) Å vs 2.972(1) Å, respectively).

A comparison of the structures of **(2)** and **(4)** indicates that the main difference is the location of the naphthyl and phenolic groups (Figure 2). In **(2)** the phenol group is further removed from the copper center than in **(4) (**2.5939(14) *vs* 2.495(2) Å, respectively), resulting in some differences related to bond angles involving the Cu-phenol bond (Table 2). With respect to the naphthalene units, Figure 2 shows that they are orthogonally positioned relative to each other.

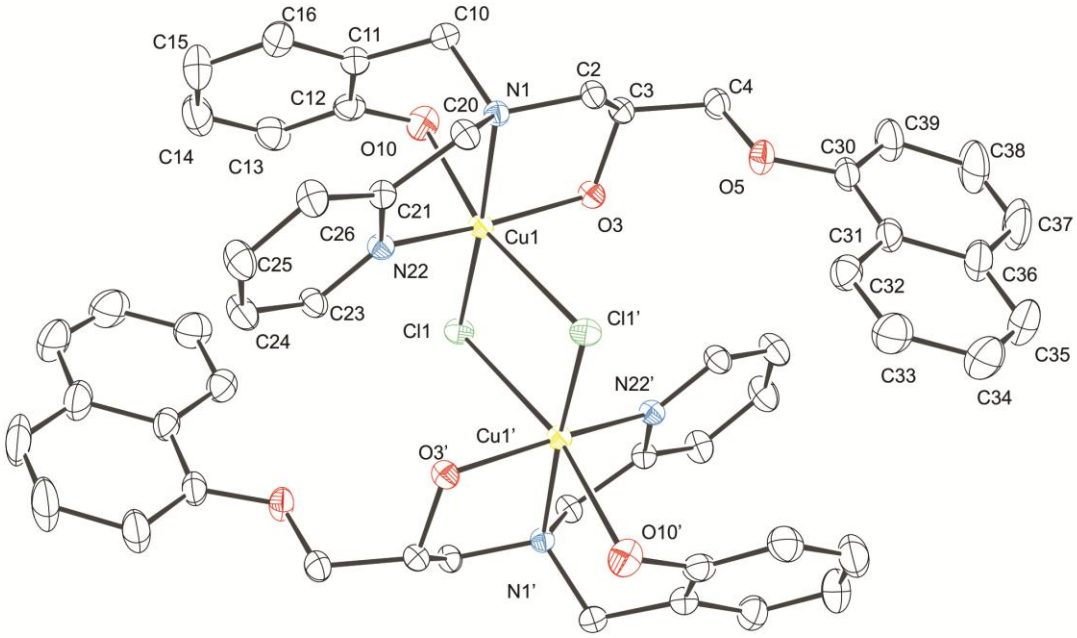

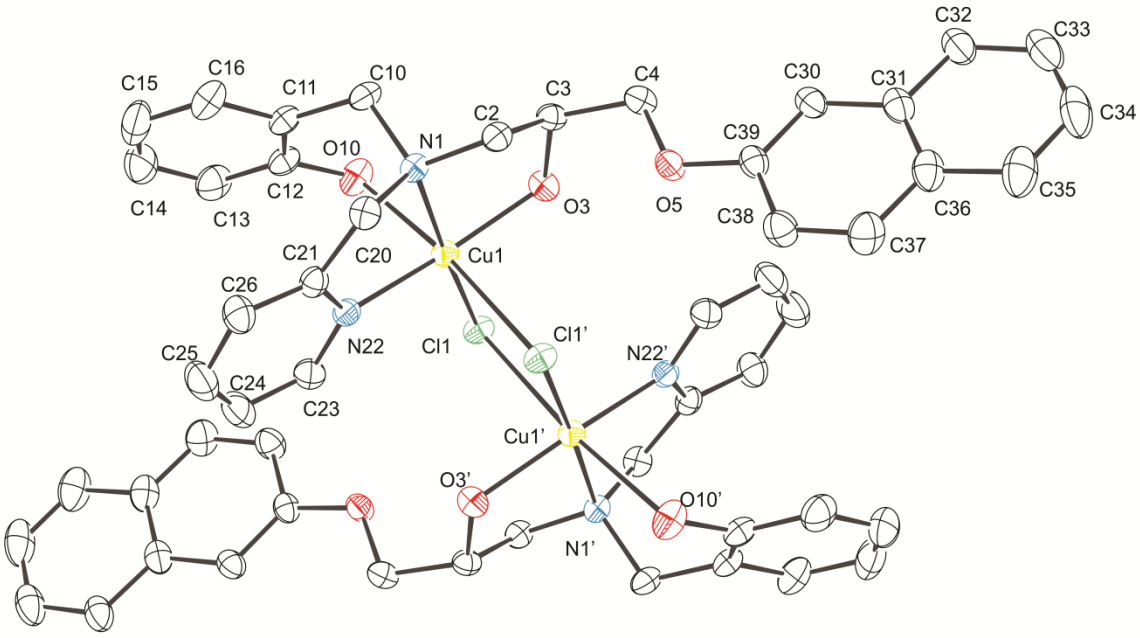

Figure 1. View of the dinuclear complexes **(2)** (top) and (**4**) (bottom) with appropriate atom labels. The ellipsoids are shown at the 40% probability level (hydrogen atoms are omitted for clarity).

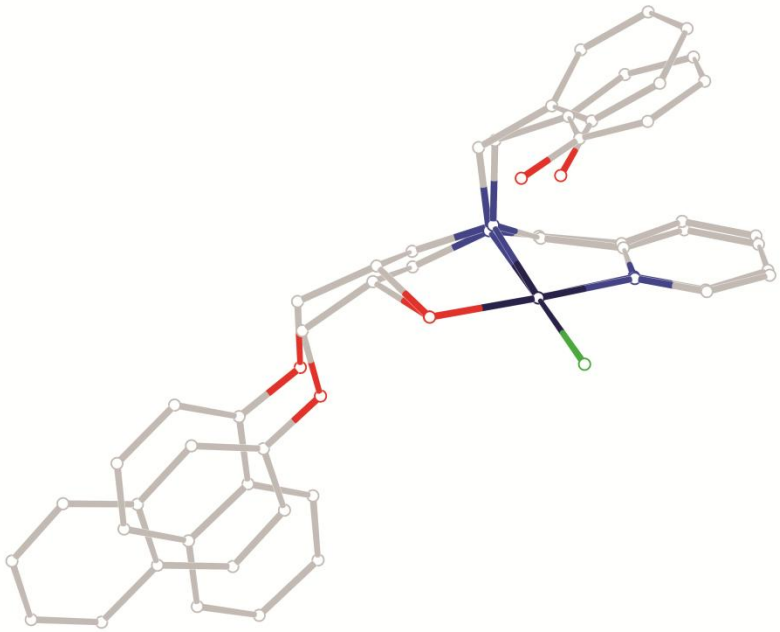

Figure 2. Overlay of the asymmetric unit of cations **(2)** and (**4**).

Table 2. Selected bond lengths [Å] and angles [º] for complexes **(2)** and **(4)**.

	Complex (**2**)	Complex **(4)**
Cu1-N22	1.9783(13)	1.991(2)
Cu1-O3	1.9824(11)	1.9854(18)
Cu1-N1	2.0374(13)	2.036(2)
Cu1-Cl1	2.2436(4)	2.2445(7)
Cu1 O10	2.5939(14)	2.495(2)
Cu1-Cl1^{i}	2.8657(4)	2.8823(8)
N22-Cu1-O3	164.01(5)	163.55(8)
N22-Cu1-N1	83.21(5)	83.25(9)
O3-Cu1-N1	84.20(5)	82.89(8)
N22-Cu1-Cl1	99.81(4)	101.35(7)
O3-Cu1-Cl1	94.02(4)	93.23(5)
N1-Cu1-Cl1	171.67(4)	173.46(6)
N22-Cu1-O10	104.74(5)	88.46(8)
O3-Cu1-O10	83.23(5)	99.40(8)
N1-Cu1-O10	82.23(5)	86.21(8)
Cl1-Cu1-O10	89.48(3)	89.26(5)
O10-Cu1-Cl1^{i}	168.03(3)	174.23(6)
N22-Cu1-Cl1^{i}	85.82(4)	85.88(6)
O3-Cu1-Cl1^{i}	85.18(4)	86.36(6)
N1-Cu1-Cl1^{i}	93.64(4)	94.28(6)

Cl1-Cu1-Cl1^{i}	94.326(13)	90.71(2)

Symmetry code: (i) -x+1,-y+1,-z+2 for complex (**2**) and (i) 1-x, 1-y, 1-z for complex (**4**)

Despite the molecular similarities, the profile of intermolecular interactions shows significant differences. The main difference is associated with the chloride ion which is in compound **(2)** connected directly to the cation while in compound **(4)** it interacts only with the methanol molecules of crystallization. The comparison between both structures indicates that the C-H$\cdots\pi$ and $\cdots\pi$ interactions in the naphthyl groups produce distortions. However, the impossibility of the description of the solvent molecules of crystallization in compound **(2)** makes it difficult to evaluate all their intermolecular interactions.

3.3. Characterization of the compounds in solution.

Since we have previously demonstrated that the dinuclear unit {[Cu^{II}(H_2BPClNOL)]–μ-$(Cl)_2$–[Cu^{II}(H_2BPClNOL)]}Cl_2 is broken into mononuclear species in polar solvents,[23] we carried out studies to evaluate the solution behavior of the copper(II) compounds synthesized in this work.

The conductivity behavior of the four complexes in MeOH was examined, revealing that they are 1:1 electrolytes. This suggests that the dinuclear arrangement observed in the solid state structures of complexes **(2)** and **(4)** may not be preserved in solution, favoring the formation of a mononuclear species instead.

ESI(+)-MS and ESI(+)-MS/MS data also indicate the presence of mononuclear species in H_2O/MeOH. ESI(+)-MS and ESI(+)-MS/MS data of complexes **(1)-(4)** present a characteristic set of isotopic ions due mainly to the presence of metal and Cl atoms. For the isomeric complexes **(1)** and **(3)**, ESI(+)-MS data indicate the presence of two cations in a MeOH:H_2O (1:1) solution. The peak at *m/z* = 497 is ascribed to [Cu(HLx)Cl]$^{+}$ (where x = 1 or 3) and the peak at *m/z* 275 may be related to the loss of

a part of the ligand. MS/MS data of the species with an *m/z* ratio of 497 yields the cation with *m/z* = 275. For the isomeric complexes **(2)** and **(4)**, four peaks were observed, *i.e.* [Cu(H2Ly)Cl]+ (*m/z* 512), $[Cu(HLy)]^+$ (*m/z* 476), H2Ly (*m/z* 415) and a peak at *m/z* 290, which is related to the fragmentation of the ligand H2Ly (where y = 2 or 4). MS/MS analysis of the species with *m/z* 512 yields a cation with *m/z* 476 (by the loss of a neutral HCl molecule) and a cation at *m/z* 290.

To extend the investigation of the behavior of the complexes in solution we carried out potentiometric titration studies of the ligands and complexes. Since biological activity generally occurs in an aqueous, buffered environment it is particularly important to assess the relevance of pH for the structure of the complexes.

For the ligand HL1, pKa values of 2.06, 2.47 and 4.64 were obtained, which are attributed to two pyridinic and one aminic nitrogen atom, respectively. The pKa values are lower than those observed for the related HPClNOL ligand (2.90(2), 3.88(2) and 4.86(2)).[35] Due to the high pKa value for the alcohol group, it remains protonated in the range from pH 0 to 13. Thus, above pH 5.0, the ligand is in its non-protonated form, *i.e.* HL1. The ligand containing the aminic nitrogen in the protonated form, $H2L1^+$, reaches a maximum of 88% at pH 3.6. The species $H3L1^{2+}$, the diprotonated species, reaches a maximum of 45% at pH 2.5. The fully protonated ligand, $H4L1^{3+}$, predominates at a pH below 2.1.

Potentiometric titration for complex **(1)**, obtained from the reaction between HL1 and $CuCl_2$, indicates that Cu^{2+} is present in its free form at pH ~ 2 and its concentration decreases gradually reaching a minimum at pH 8.5., when the metal ion is coordinated by HL1, reaching a maximum of 90% in the range of pH 5-7.5. At pH values higher than 9, two species associated with two deprotonation/protonation equilibria involving one water molecule and the alcohol group are observed: $[Cu(HL1)Cl(OH)]^0$ and $[Cu(L1)Cl(OH)]^-$, with pKa values of 9.35 and 9.89, respectively. The hydrolysis product of the metal ion appears at higher pH values. Similar results were obtained for

ligand HL3 and its copper complex [Cu(HL3)Cl]Cl.2H_2O **(3)**, since HL1 and HL3 are isomers.

For the ligand H2L2 pKa values of 1.71, 4.97 and 11.49 were obtained and attributed to one pyridinic group, one aminic group and one phenolic group, respectively. The species containing the phenol in the protonated form (H2L2) reaches a maximum in the range between pH 6.5 and 11 (Figure 3). The deprotonation of the alcohol group was not observed in the pH range investigated.

Potentiometric titration of complex **(2)**, obtained from the reaction between H2L2 and $CuCl_2$, indicates Cu^{2+} is in its free form at pH ~ 2 and its concentration decreases until pH 6.5 (Figure 4). Consequently, the coordination of Cu^{2+} with H2L2 is observed from pH 2.0 upwards, and reaches a maximum of 99% at pH 7.0 (species E1: $[Cu(H2L2)Cl(OH_2)]^+$, with a pKa of 7.2). At higher pH values two species associated with two deprotonation/protonation equilibria, involving one water molecule and the phenol group, respectively, were observed: $[Cu(H2L2)Cl(OH)]^0$ (species E2) and $[Cu(HL2)Cl(OH)]^-$ (species E3), with pKa values of 9.24 and 11.4. At a pH higher than 11 the Cu^{2+} is completely hydrolyzed. As anticipated similar results were obtained for the isomeric ligand H2L4 and its copper complex [(H2L4)Cu(μ-Cl)$_2$Cu(H2L4)]Cl_2.6H_2O (4).

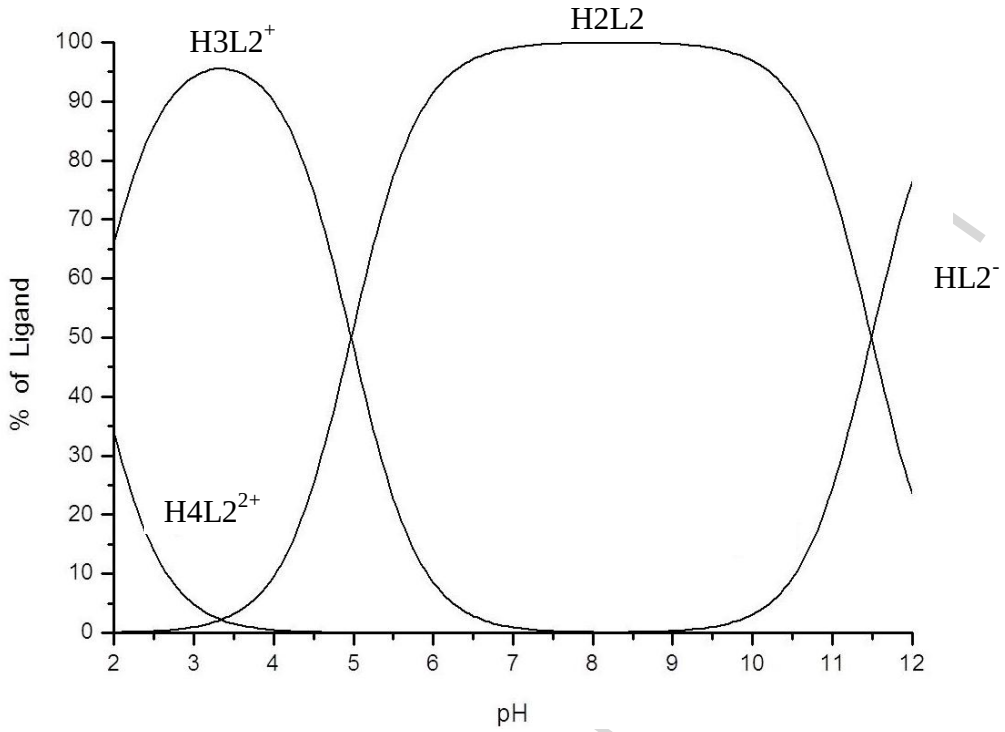

Figure 3. Relative concentrations of the ligand H2L2 as function of the pH, calculated from potentiometric titration data. H4L2: the pyridinic nitrogen, aminic nitrogen, phenol and alcohol groups are protonated; H3L2: the aminic nitrogen, the alcohol and phenol groups are protonated; H2L2: the phenol and the alcohol groups are protonated. $HL2^-$: the phenol group is deprotonated. The alcohol group remains protonated in the range from pH 0 to 13.

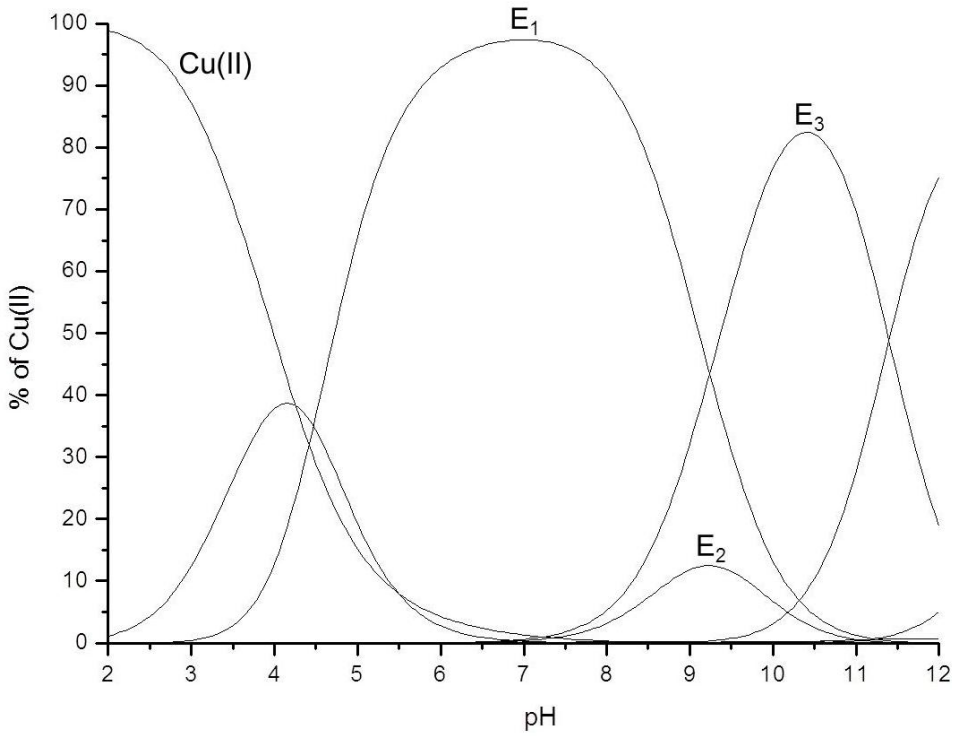

Figure 4. Relative concentrations of the copper complexes as a function of pH for a supersaturated solution, calculated from potentiometric titration data for complex **(2)**. E1: $[Cu(H2L2)Cl(OH_2)]^+$, E2: $[Cu(H2L2)Cl(OH)]^0$ and E3: $[Cu(HL2)Cl(OH)]^-$.

Based on the potentiometric titration, the species $[Cu(H2L2)Cl(OH_2)]^+$ reaches its maximum concentration at pH 7.0 and is the main species in the range from pH 4.5 to 9.2.

Thus, in summary, the three techniques presented above indicate that the dinuclear unit is broken into monomeric species in solution. Based on potentiometric titration studies, at physiological pH, the main species for complexes **(1)** and **(3)** is $[Cu(HL)(H_2O)]^{2+}$, and $[Cu(H2L)(H_2O)]^{2+}$ for complexes **(2)** and **(4).**

3.4. Spectroscopic characterization.

The IR spectra of complexes **(1)-(4)** were analyzed and compared to those of their common free ligands HL1-H2L4 in the region 4000-400 cm^{-1}. For ligand HL1, characteristic bands of the aromatic

group are observed at 1589, 1508, 1435, 791 and 771 cm^{-1}, assigned to $\nu_{C=N}$, $\nu_{C=C}$ and $\delta_{(pyridine\ ring)}$, respectively. For ligand H2L2, these bands are observed at 1581, 1482, 1400, 791 and 756 cm^{-1}. There is a band at 1242 cm^{-1}, attributed to the phenol group (ν_{C-O}). For ligand HL3 and H_2L4, bands similar to those of HL1 and H2L2, respectively, are observed.

The electronic spectra for ligands HL1 and HL3, in acetonitrile, are also similar and display four distinct bands in the range between 210 to 295 nm, which are attributed to a $\pi \rightarrow \pi^*$ intraligand transition due to the high value of ε. Similar bands are also observed for complexes **(1)** and **(3)**. In addition, the complexes also have transitions in the visible range. These bands at 707 nm (ε: 77 dm^3 mol^{-1} cm^{-1}) and 702 nm (ε: 69 dm^3 mol^{-1} cm^{-1}) for **(1)** and **(3)**, respectively, are attributed to d-d-transition.

For ligands H2L2 and H2L4 and their corresponding complexes several bands were observed in the range between 210 and 320 nm, which are again attributed to $\pi \rightarrow \pi^*$ intraligand transitions. Complex **(2)** has additional two bands at lower energy (at 444 nm (18 $dm^3.mol^{-1}.cm^{-1}$) and 721 nm (72 $dm^3.mol^{-1}.cm^{-1}$)), while **(4)** has two corresponding bands at 440 nm (ε: 29 $dm^3.mol^{-1}.cm^{-1}$) and 732 nm (ε: 68 $dm^3.mol^{-1}.cm^{-1}$), all of which are attributed to d-d transitions.

EPR spectra for complexes **(1)-(4)** show only a signal typical of Cu^{2+} in an axial symmetric environment, with a $3d^9$ electronic configuration and S = 1/2. The nuclear spin for both ^{63}Cu (natural abundance 69%) and ^{65}Cu (natural abundance 31%) isotopes is I = 3/2. Therefore, 2I + 1 = 4 perpendicular and parallel hyperfine components can be expected, resulting from the dipole-dipole interactions between the magnetic moments of the nucleus and the electronic moments of the paramagnetic ion. The EPR spectra for **(1)-(4)** are shown in Figure 5 and Table 3 lists the parameters obtained from the corresponding simulations. The spectra were simulated using the electronic Zeeman and the hyperfine interactions, which are typical for mononuclear copper complexes.[36] Usually, the interaction of the nuclear quadrupole moment with the electrical field gradient is very small and can be

ignored.[37] For transition metal ions in which the d shell is more than half full, like Cu^{2+}, g-factors greater than that for the free electron (2.0023) are expected.[38] According to Kivelson and Neiman the value of $g_{//}$ is related to the nature of the environment; $g_{//}$ greater than 2.3 indicates an ionic environment, while $g_{//}$ less than 2.3, as is the case for each system studied here, indicates a rather covalent interaction between the metal and its ligands.[39] Furthermore, in all the recorded spectra $g_{//}>g_{\perp}>2.0023$ and $A_{//}>A_{\perp}$, which indicates that the Cu^{2+} ions are located in distorted octahedral sites (D_{4h}) with an elongated z-axis; the ground state is characterized by the term $^2B_{1g}$.[40] Complexes **(1)** and **(3)**, which contain the group bis(2-picolyl)amine, have the lowest $g_{//}$ values and a stronger hyperfine interaction (larger $A_{//}$**)**, due to the presence of three N donor groups in the copper coordination sphere. Complexes **(2)** and **(4)**, which have the group 2-(hydroxybenzyl)(2-pyridylmethyl)amine instead, exhibit weaker hyperfine interactions (smaller $A_{//}$) and weaker interactions between the magnetic moments of the nucleus and unpaired electron.

Table 3. Summary of the spin Hamiltonian parameters obtained from simulations of the experimental EPR spectra recorded for complexes **(1)-(4)**.

Compound	$\mathbf{g_{//}}$ (±0.001)	$\mathbf{g_{\perp}}$ (±0.004)	$\mathbf{A_{//}}$ **(MHz)** (±5)	$\mathbf{A_{\perp}}$ **(MHz)** (±5)
(1)	2.242	2.055	540	20
(3)	2.242	2.060	540	27
(2)	2.273	2.065	520	30
(4)	2.275	2.063	520	20

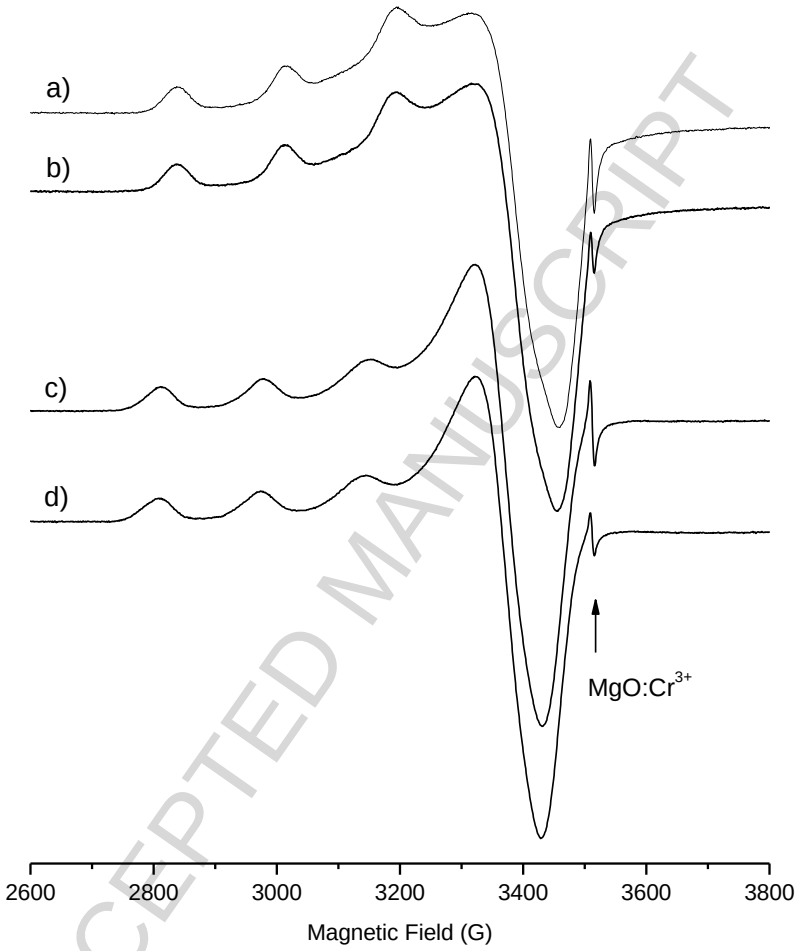

Figure 5. EPR spectra of the copper complexes (a) **(1)**, (b) **(3)**, (c) **(2)** and (d) **(4)** in DMSO at 100 K. $MgO:Cr^{3+}$ (g=1.9797) was used as a reference signal.

3.5. Electrochemical Studies.

Cyclic voltammetry was employed in the electrochemical characterization of the copper complexes **(1)-(4).** The cyclic voltammogram for isomers **(1)** and **(3)** shows one *quasi* reversible redox process at $E_{1/2}$ = -0.324 and -0.348 V *vs* NHE, respectively. In the compound [Cu(HPClNOL)Cl]Cl, whose ligand is similar to HL1 and HL3, but instead of the naphthyl group contains a chloride, the observed $E_{1/2}$ value was -0.172 V *vs* NHE.[21] This difference in the redox potential indicates that the

ligands HL1 and HL3 are better donors than the ligand HPClNOL. The presence of just one redox process suggest the presence of mononuclear species in CH_3CN solution, in agreement with other in solution studies described above.

Complexes **(2)** and **(4)**, as a result of their structural similarity, have one cathodic process at 0.164 and 0.114 V *vs* NHE, and one anodic process at -0.588 and -0.538 V vs NHE, respectively. The two redox processes are far apart, indicating an irreversible electrochemical behavior.[41,42] The cathodic process is attributed to the Cu(II)/Cu(I) couple with the concomitant loss of the chloride ligand, resulting in a tetracoordinated Cu(I) complex. The anodic process is due to the oxidation of the Cu(I) complex, resulting in a pentacoordinated Cu(II) complex. The presence of one pyridine and one phenol in the structure of the ligands H2L2 and H2L4 seems to facilitate the release of the chloride ligand from the coordination sphere after the reduction of the copper(II) center. In contrast, the presence of two pyridine groups in the ligands HL1 and HL3 appears to facilitate the retention of the coordination sphere, avoiding the release of the chloride ligand. Figure 6 shows the cyclic voltammogram for complex **(4)**.

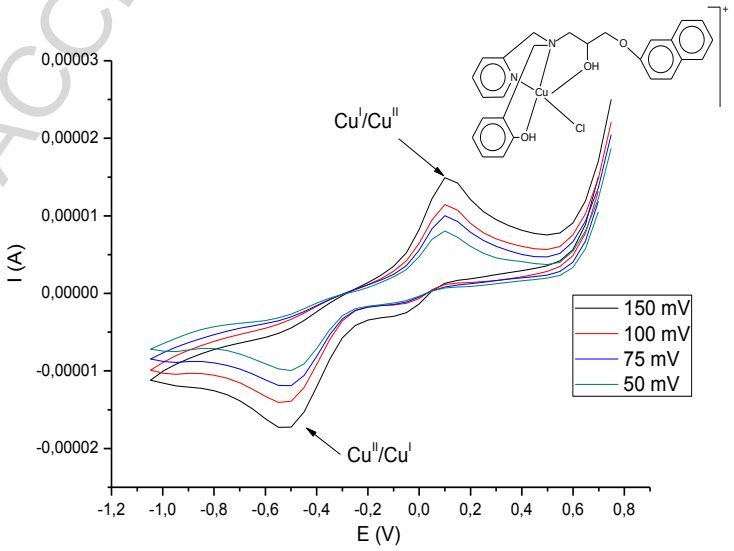

Figure 6. Cyclic voltammogram of complex **(4)**. The inset shows the proposed structure of the mononuclear species.

3.6. Assessment of cell viability by MTT Assay.

The screening of the anti-growth effect of new biologically active compounds is essential in cancer research with regard to the development of novel antitumor drugs. Here, the cytotoxicity of the complexes was assessed using human leukemia cell lines (U937 and THP-1) and PBMC by means of the colorimetric MTT assay which is based on the conversion of the yellow tetrazolium salt MTT to purple formazan crystals by metabolically active cells (see Figure 7).[43] For comparative purposes, the cytotoxicity of cisplatin for PBMC was also evaluated under the same experimental conditions. As presented in Table 4, complex **(2)** exerts a potent inhibitory effect on the growth of THP-1 and U937 cell lines, with IC_{50} = 11.30 (THP-1) and 8.20 μmol dm^{-3} (U937). Importantly, these values are lower than those obtained for cisplatin (11.84 and 16.25 μmol dm^{-3}, respectively). The anti-tumor activity of the corresponding ligands (HL1, H2L2, HL3 and H2L4) is, in most cases, lower than that of their respective copper(II) complexes. The exceptions are HL1 and HL3 when tested for their effect on the U937 cell line. In general, for all the ligands and corresponding coordination compounds, the α-isomers were more active than the β-isomers, and the compounds containing a phenol moiety were more active than compounds without this group (Table 4). Only complexes **(2)** and **(4)** have an inhibitory effect on PBMC cells (IC_{50} = 16.35 and 36.25 μmol dm^{-3}, respectively); for comparison, the IC_{50} of cisplatin is 37.5 μmol dm^{-3}. Thus, apart from H2L4 (low solubility) the naphthyl-containing ligands (HL1 – HL3) and their corresponding copper complexes (**1 - 4**) have a significantly greater susceptibility for human leukemia cell lines THP-1 and U937. This observation highlights the influence of the naphthalene backbone on the antitumor activity toward the leukemic cell lines under investigation (THP-1 and U937), since for a similar compound in which this structural feature is absent, *i.e.* $[Cu(HPClNOL)Cl]^{+}$, the activity is significantly lower.[21]

Table 4. The 50% Inhibitory Concentration (IC_{50}) of copper complexes and their respective ligands for human leukemia cell lines (THP-1 and U937) and PBMC.

Compounds	IC_{50}/µmol dm^{-3}		
	THP-1	U937	PBMC
HL1	43.67 ± 1.09	32.22 ± 1.11	> 100
(1)	30.72 ± 1.09	58.51 ± 1.09	79.64 ± 1.1
H2L2	66.97 ± 1.07	30.95 ± 1.06	> 100
(2)	11.30 ± 1.06	8.20 ± 1.04	16.35 ± 1.11
HL3	87.79 ± 1.09	38.56 ± 1.17	> 100
(3)	25.44 ± 1.07	54.75 ± 1.19	86.99 ± 1.13
H2L4	> 100	> 100	> 100
(4)	34.03 ± 1.04	39.34 ± 1.04	36.25± 1.10
Cisplatin	11.84 ± 1.05	16.25 ± 1.05	37.50 ± 1.13
$CuCl_2$. $2H_2O$	>100	>100	>100

* SD indicates the standard error of the mean. The cytotoxicity of the complexes was determined after 36 h of incubation, using the MTT method.[43] *Data represent the mean of triplicate measurement which was repeated twice.

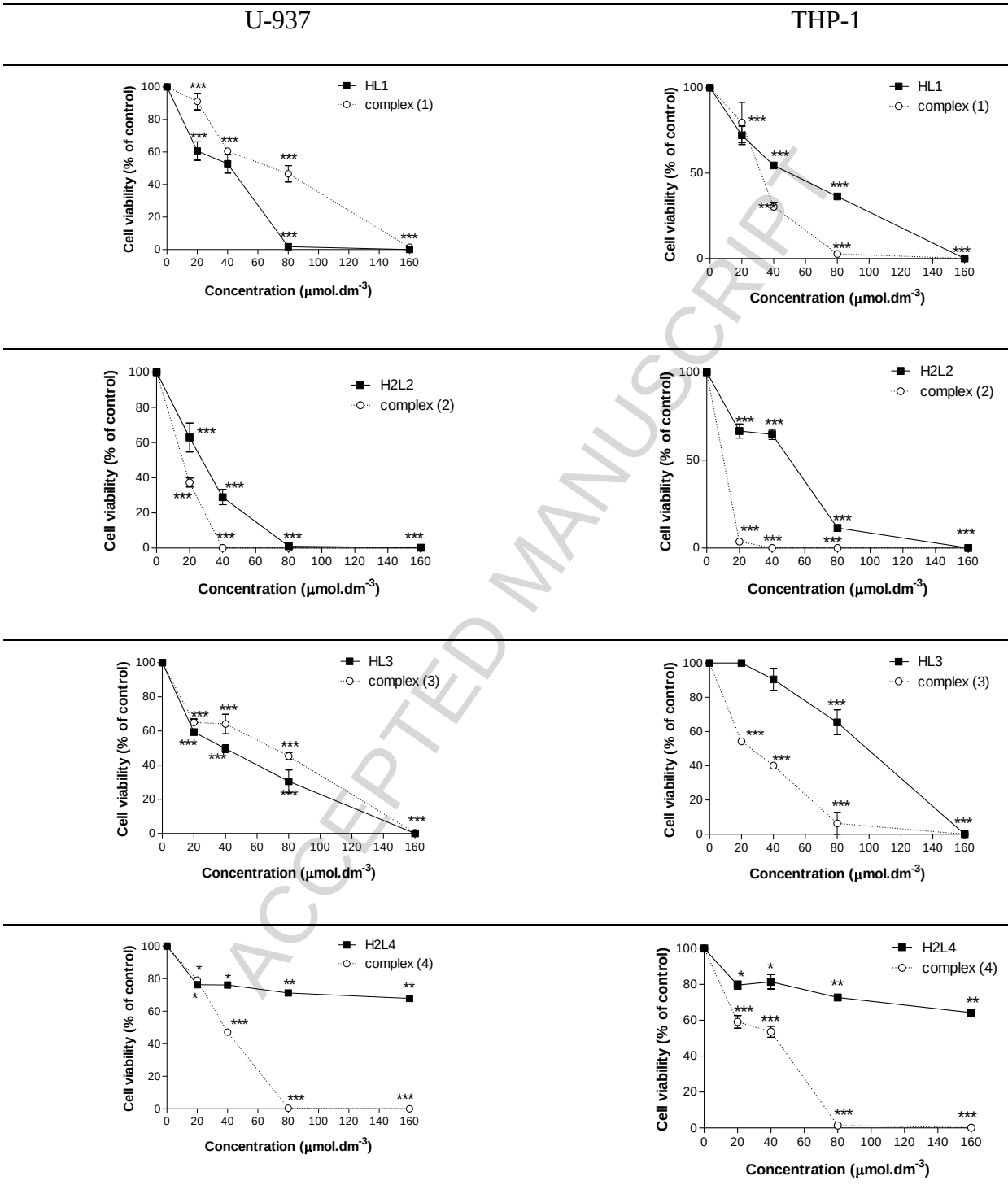

Figure 7. Cytotoxicity of ligands HL1 - H2L4 and their corresponding copper complexes **(1) - (4)**, tested against human leukemia cell lines U-937 and THP-1. Dose-response curves were obtained using the MTT assay after 36 h of exposure. Each data point represents the means ± S.D. (n = 3). *P < 0.05, **P < 0.01 and ***P < 0.001 *versus* control.

In summary, the IC_{50} values obtained in this work, especially for complex **(2)** against U937 (~8 μmol dm^{-3}), are similar to those previously reported in the literature, under same experimental conditions. However, these values are higher than reported for conventional antineoplastic agents, such as cytarabine, doxorubicin and vincristine.[44]

3.7. In vivo acute toxicity for complex (2) - LD_{50}.

Complex **(2)** showed the highest activity/toxicity toward the studied cancer cells, but it was more toxic to normal cells than cisplatin (Table 4). We thus decided to investigate the *in vivo* acute toxicity of **(2)**, and compare with corresponding data available for cisplatin. C57BL/6 mice, 4-5 weeks old, were divided into groups of four animals for each treatment condition. The concentrations of complex **(2)** used were 13.75, 27.50, 55 and 110 mg kg^{-1}. Figure 8 shows the percentage of live animals in relation to increasing concentrations of the complex. The LD_{50} (median lethal dose that killed 50% of animals) for complex **(2)** was 55 mg kg^{-1} *versus* 14.51 mg kg^{-1} for cisplatin.[45] These data indicate that complex **(2)**, although more toxic to normal cells (PBMC) than cisplatin, is less toxic than cisplatin *in vivo*. This is an encouraging observation, insinuating that complex **(2)** may be safer and more effective than an approved drug.

Figure 8. Determination of the *in vivo* acute toxicity (LD_{50}) of complex **(2)**. Animals were inoculated intraperitoneally with various concentrations of the compound. The figure shows the percentage of live animals relative to the concentration of complex **(2).**

3.8. Mechanistic Studies of Cell Death.

The encouraging LD_{50} value obtained for compound **2** prompted us to investigate the effects exerted by the compounds on cancer cells in more detail. While the MTT method assesses quantitatively cell viability, it cannot distinguish between apoptosis or necrosis. Based on the cytotoxicity assessment above (Table 4), the most promising molecules (H2L2, **(2)** and **(4)**) were selected to investigate the mechanism by which they induce cell death in leukemic cell lines. Apoptosis or programmed cell death is a complex cellular process which comprises morphological changes such as shrinkage of the cytoplasm, nuclear condensation, blebbing and formation of apoptotic bodies. Apoptosis is a type of cell death which plays an important role in tissue homeostasis since it is responsible for the deletion of cells in normal tissues. However, apoptosis also occurs in pathological processes and has been shown to be responsible for the normal elimination of cells with damaged DNA. Dysregulation of apoptosis leads to a variety of human pathologies including cancer, autoimmune diseases and neurodegenerative disorders.[46] It is thus important to understand the molecular mechanism of cell death promoted by coordination compounds in order to establish

structure/activity relationships that may assist the development of new antitumor drugs. Here, the function of ligand H2L2 and complexes **(2)** and **(4)** in apoptosis were investigated by (i) fluorescence microscopy, (ii) flow cytometric analysis of cell cycle arrest and (iii) an analysis of mitochondrial membrane potentials ($\Delta\Psi m$). Furthermore, for complex **(2)** its effect on apoptosis was assessed by Annexin V-FITC/PI analysis, DNA fragmentation and agarose gel electrophoresis, subcellular fractionation and detection of cytochrome C release, determination of caspase activities, and an analysis of the mitochondrial morphology by fluorescence imaging and transmission electron microscopy (TEM).

3.9. Fluorescence microscopy.

The determination of the percentage of apoptotic cells was carried out by fluorescence microscopy using acridine orange/ethidium bromide double staining. Compounds H2L2, **(2)** and **(4)** significantly increased the proportion of apoptotic cells over the evaluated time. Figure 8 shows only the results obtained against U937 cells. Ligand H2L2 and complexes **(2)** and **(4)** induced stronger apoptotic response in both cells lines (THP-1 and U937) in a dose and time dependent-manner. Extensive cell death by apoptosis for both cell lines was promoted by complex **(2)** at a concentration of 40 μmol dm^{-3} after 12 h incubation. After treatment, U937 cell lines showed changes in their morphology in form of chromatin condensation and nuclear fragmentation (Figure 9). It is thus likely that the growth inhibition of human leukemia cell lines induced by the ligands and copper compounds (determined by the colorimetric MTT method; see above) is associated with the induction of apoptosis.

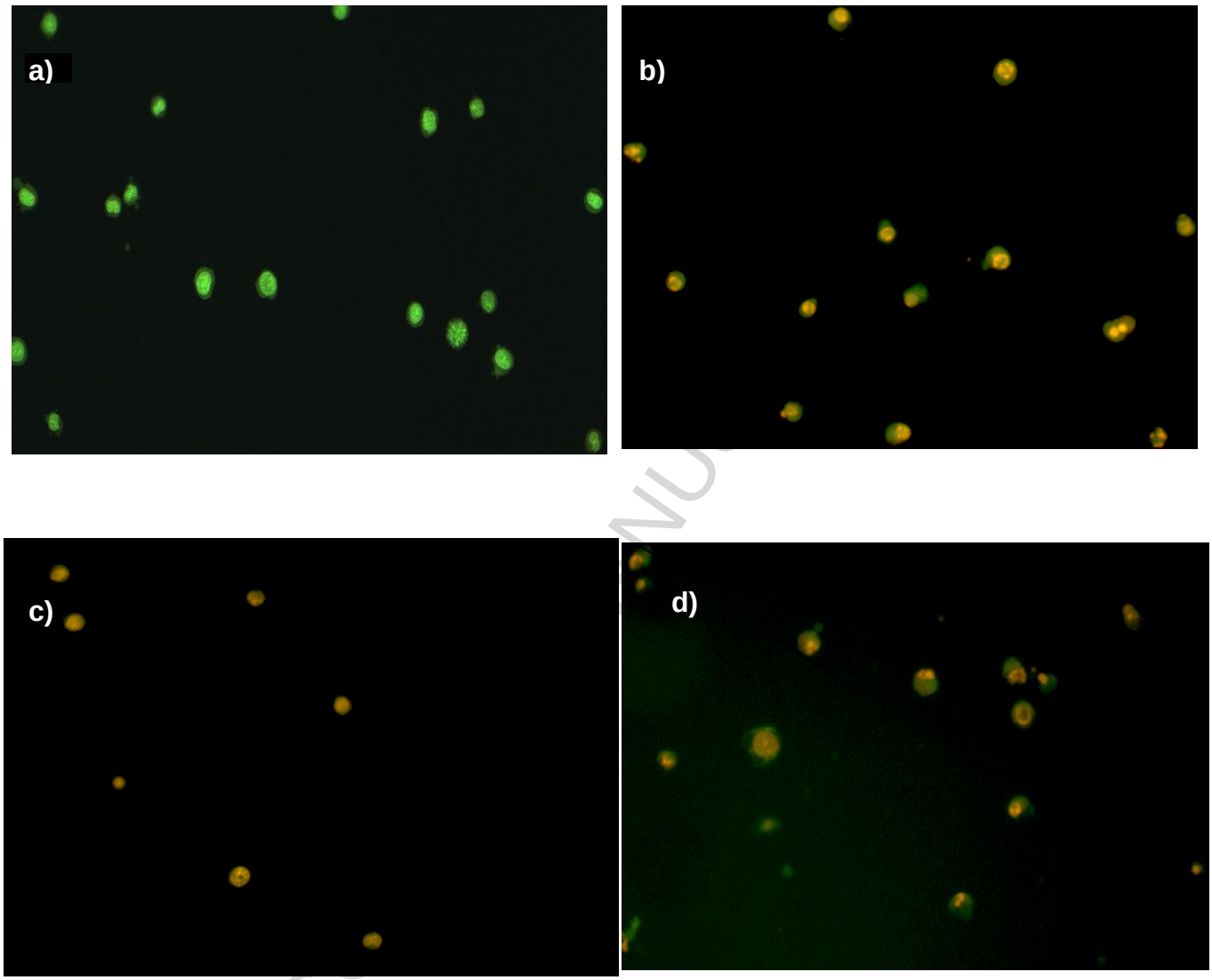

Figure 9. Morphological investigation employing fluorescence microscopy of the U937 leukemia cell line, after treatment with ligand H2L2 and complexes **(2)** and **(4)**. a) Control cells. b) Cells after 36 h treatment with 40 μmol dm^{-3} of complex **(2)**. c) Cells after 36 h treatment with 80 μmol dm^{-3} of complex **(4)** and d) cells after 36 h treatment with 80 μmol dm^{-3} of ligand H2L2.

3.10. Measurement of apoptosis by Annexin V-FITC/PI analysis.

In order to confirm and quantify the extent of apoptosis, a double-labeling technique using annexin V-FITC and propidium iodide (PI) was utilized. This technique is based on the phosphatidyl-

serine externalization. Phosphatidyl-serine is predominantly accumulated in the inner plasma membrane of living cells, but in the apoptotic cells this compound is translocated from the inner to the outer plasma membrane. In the flow cytometric analysis (Figure 10) the histogram in the lower left quadrant (negative for annexin V and PI) is regarded as the population of live cells (normal), the one in the lower right quadrant (positive for annexin V and negative for PI) illustrates the cell population at the early apoptotic stage, while the upper right quadrant (positive for annexin V and PI) and the upper left quadrant (negative for annexin V and positive for PI) represent the cell population at the late apoptotic stage and the necrotic cell population, respectively. Figure 10 shows that after 12 h of treatment with 80 μmol dm^{-3} of complex **(2)**, approximately 27% of U937 and 8% of THP-1 cells were in an early apoptotic stage and ~72% of U937 and ~91% of THP-1 cells were in the late stage of apoptosis. Only ~1% of the cell populations were still normal. At lower concentrations of complex **(2)** (40 μ μmol dm^{-3}) the normal cells still form the major proportion in the respective cell cultures but already approximately one third of the cell population has reached a late apoptotic stage for both U937 and THP-1. Thus, in summary, the results from MTT, fluorescence microscopy and the Annexin V-FITC/PI analysis consistently indicate that complex **(2)** effectively induces apoptosis in THP-1 and U937 cell lines in a dose-dependent manner.

3.11. Detection of Apoptosis by DNA Fragmentation and Agarose Gel Electrophoresis.

DNA fragmentation is a key feature of the apoptosis process, largely due to the activation of endogenous endonucleases (such as caspases) which subsequently induce cleavage of chromatin DNA into internucleosomal fragments of roughly 180 base pairs. Monitoring the pattern of DNA fragmentation by agarose gel electrophoresis is thus a qualitative way to assess apoptosis.[47] The gel pattern of the DNA samples isolated from untreated control U937 and THP-1 cells shows intact DNA bands (retained at the top of the gel), whereas the gel pattern of the DNA samples isolated after

treatment with complex **(2)** shows degraded DNA bands in the form of ladders (Figure 11). Thus, in agreement with the studies described above, the presence of these ladders strongly suggests that the treatment with complex **(2)** promotes apoptosis in both human leukemic cell lines.

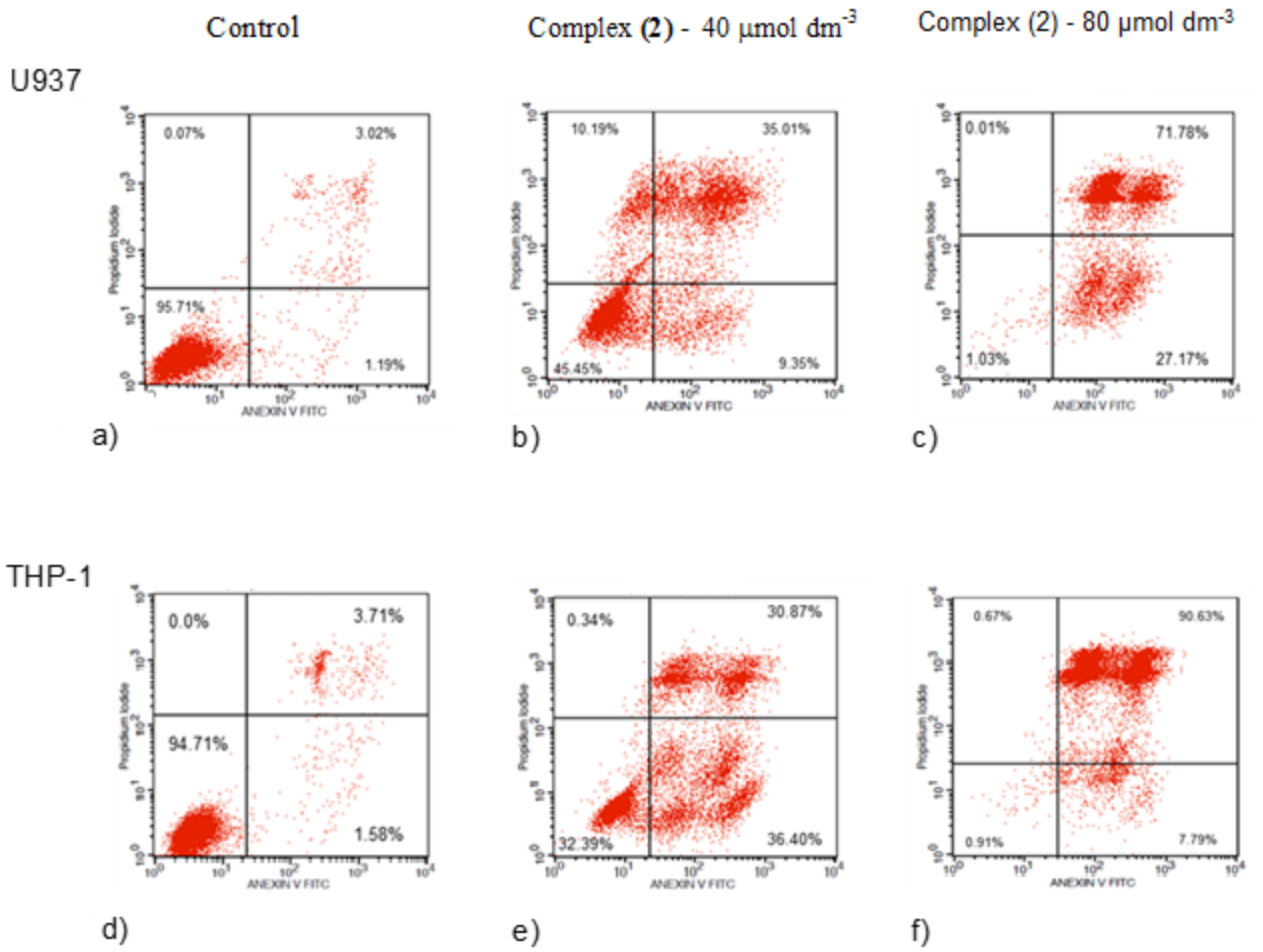

Figure 10. Annexin V-FITC/PI staining of THP-1 and U937 cells after treatment for 12h with complex **(2)**. a) U937 (control), b) U937 cells after treatment at a concentration of 40 µmol dm^{-3} of complex **(2)**, c) U937 cells after treatment at a concentration of 80 µmol dm^{-3} of complex **(2)**, d) THP-1 (control), e) THP-1 cells after treatment at a concentration of 40 µmol dm^{-3} of complex **(2)**, f) THP-1 cells after treatment at a concentration of 80 µmol dm^{-3} of complex **(2)**. The data are presented in dot blots depicting annexinV/FITC *versus* PI staining. The percentages of cells in each quadrant is indicated.

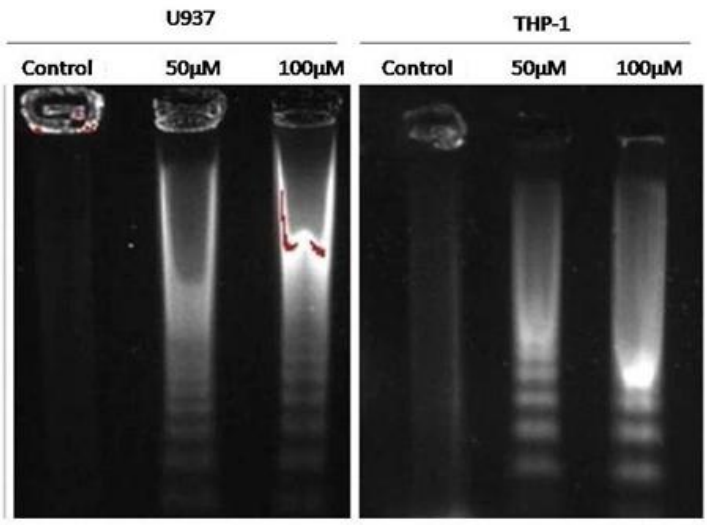

Figure 11. Gel patterns of DNA samples isolated from untreated control U937 and THP-1 cells and cells after treatment with complex **(2)** (50 and 100 μmol dm^{-3}). The DNA ladder formation following the treatment with **(2)** indicates induction of apoptosis in both human leukemic cell lines.

3.12. Cell cycle arrest by flow cytometric analysis.

The *in vitro* quantification of the relative cellular DNA content from leukemic cell suspension cultures by flow cytometry enables the identification of the cell distribution during the various phases of the cell cycle (*i.e.* G_1, S-DNA synthesis, G_2 and M-mitosis) and is a powerful method to investigate the mechanism of cell death. Consequently, the relative cellular DNA content and distribution during the various phases of the cell cycle after 36 h of incubation with the biologically most active compounds generated in this work (*i.e.* ligand H2L2 and complexes **(2)** and **(4)**) were determined by flow cytometry (Figure 12). The results demonstrate that the populations of leukemia cell lines (THP-1 and U937) in each phase of their cell cycles were affected by treatments with these compounds. The G1

phase, also called growth phase as it ensures that the cell is primed for DNA synthesis, plays a crucial role in cell cycle progression. As shown in Figure 12, the population of THP-1 cells in the G1 phase changed from ~60% in the control to ~3% (after treatment with 80 μmol dm^{-3} H2L2) and ~17% (after treatment with 40 μmol dm^{-3} of either **(2)** or**(4)**). For the U-937 cell line the corresponding values are ~67% (control), 0.32% (H2L2), ~3.5% (**(2)**) and ~20% (**(4)**), demonstrating a significant decrease in the population of cells in the G1 phase. It is also worthwhile noting that the population of cells in the sub-G1 phase, for both leukemia cell lines, increased significantly upon these treatments (Figure 12). The marked increase of cell populations in the sub-G1 phase corresponds to cells whose DNA has been cleaved by cellular nucleases that were activated by the apoptosis machinery. Thus, the compounds under investigation inhibit the growth and hinder the proliferation of THP-1 and U937 cells, and these effects are related directly to cell cycle arrest. This interpretation is in agreement with studies on a ternary copper(II) complex with cytotoxic activity against cancer cells[48] and a Schiff base copper(II) complex associated with the cell cycle arrest of MCF-7 cells (human cancer cell line).[49]

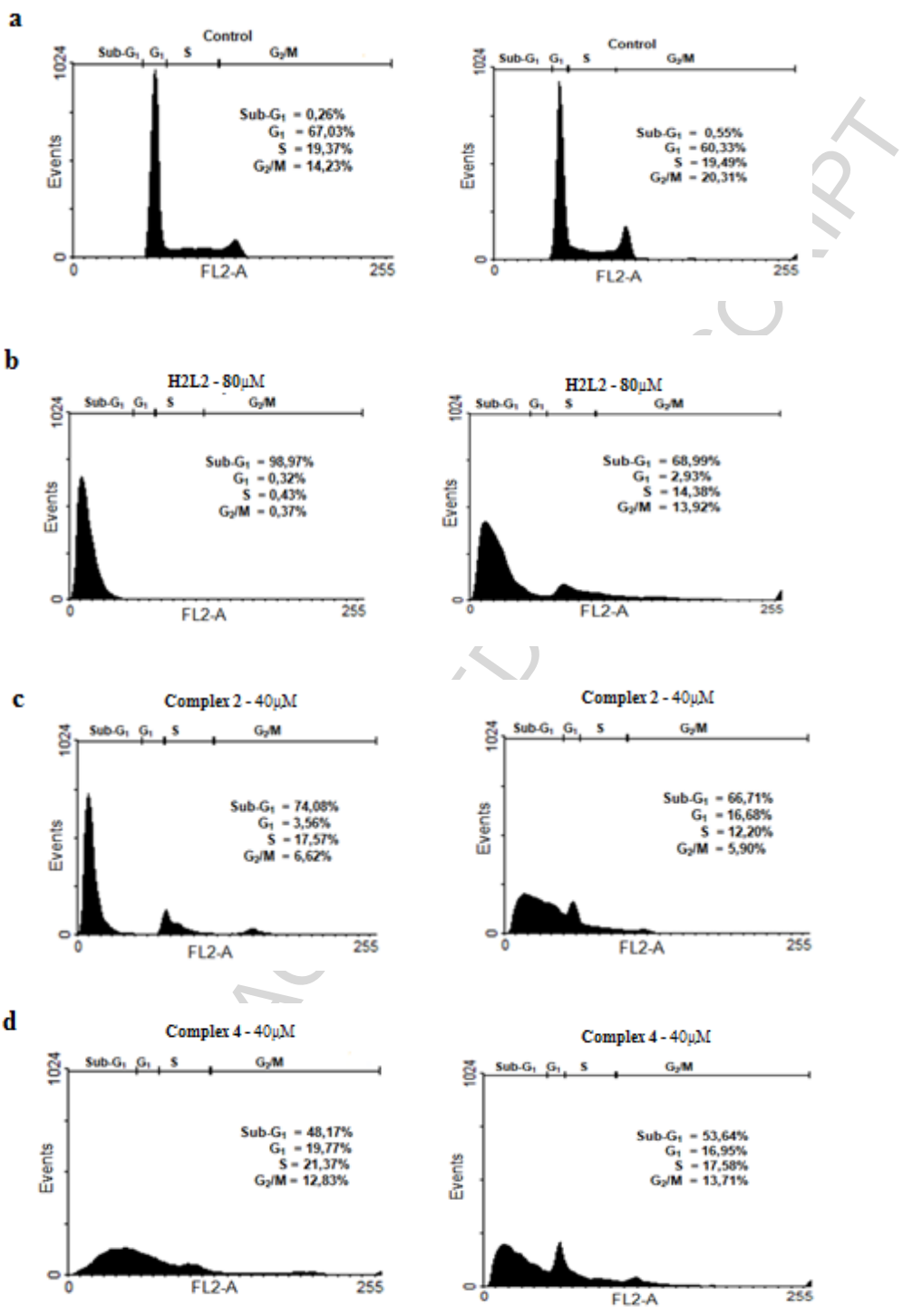

Figure 12. Cell cycle analysis by flow cytometry. Leukemic cells lines (U937 and THP-1) were stained with propidium iodide (PI) after 36 h of incubation without (Control) and with the ligand H2L2 and complexes **(2)** and **(4)**. Cells with hypodiploid DNA content were measured by quantifying the sub-G_1

peak in the cell cycle pattern. Each experiment was carried out by recording 10,000 events. (a) Control cells; (b) cells after treatment with 80 μmol dm^{-3} H2L2; (c) cells after treatment with 40 μmol dm^{-3} **(2)**; (d) cells after treatment with 40 μmol dm^{-3} **(4)**.

3.13. Analysis of mitochondrial membrane potential potential (ΔΨm) and cytochrome C release.

The mitochondrial membrane potential (ΔΨm) is an important parameter for mitochondrial function, and is also used as indicator of cell death.[50] Loss of mitochondrial membrane potential (ΔΨm) is a characteristic marker for apoptosis and it is an early event coinciding with cytochrome *c* and caspase activation. The lipophilic cationic dye 5,5',6,6'-tetrachloro-1,1',3,3'-tetraethylbenzimi-dazolylcarbocyanine iodide (JC-1) can selectively enter mitochondria and reversibly change color from red to green as the membrane potential decreases. In healthy cells, with high mitochondrial membrane potential, JC-1 spontaneously forms complexes known as J-aggregates with intense red fluorescence, detectable by flow cytometry. In contrast, in apoptotic or unhealthy cells with low ΔΨm, JC-1 remains in the monomeric form, characterized by green fluorescence.[51] As shown in Figure 13 (quadrant C), control cells of THP-1 and U937 show a strong red fluorescence (93.7 and 96.4%, respectively) after staining with JC-1. Following treatment with 80 μmol dm^{-3} ligand H2L2 for 36 h the red fluorescence decreased to ~39% and ~1% for THP-1 and U937 cells, respectively. The corresponding values following treatments with 40 μmol dm^{-3} of **(2)** and 80 μmol dm^{-3} of **(4)** were 3.7% and 11.4%, and 10.5% and 2.3% for THP-1 and U937 cell lines, respectively (Figure 13). Thus, each of the treatments above leads to a collapse of ΔΨm. Concomitant with the observed decrease in red fluorescence in quadrant C is an increase in green fluorescence in quadrant D. These results are in good agreement with those obtained from the MTT assay (Table 4 and Figure 7), and demonstrate that the toxicity of the compounds under investigation against leukemic cell lines is mediated via apoptosis, being directly related to mitochondrial dysfunction. The loss of mitochondrial the membrane potential is believed to

occur through the formation of pores in the mitochondria accompanied by the release of cytochrome *c* into the cytoplasm.[51] Indeed, upon treatment of U937 cells with **(2)** cytochrome *c* release from the mitochondria into the cytosol was observed in a time-dependent manner (Figure 14).

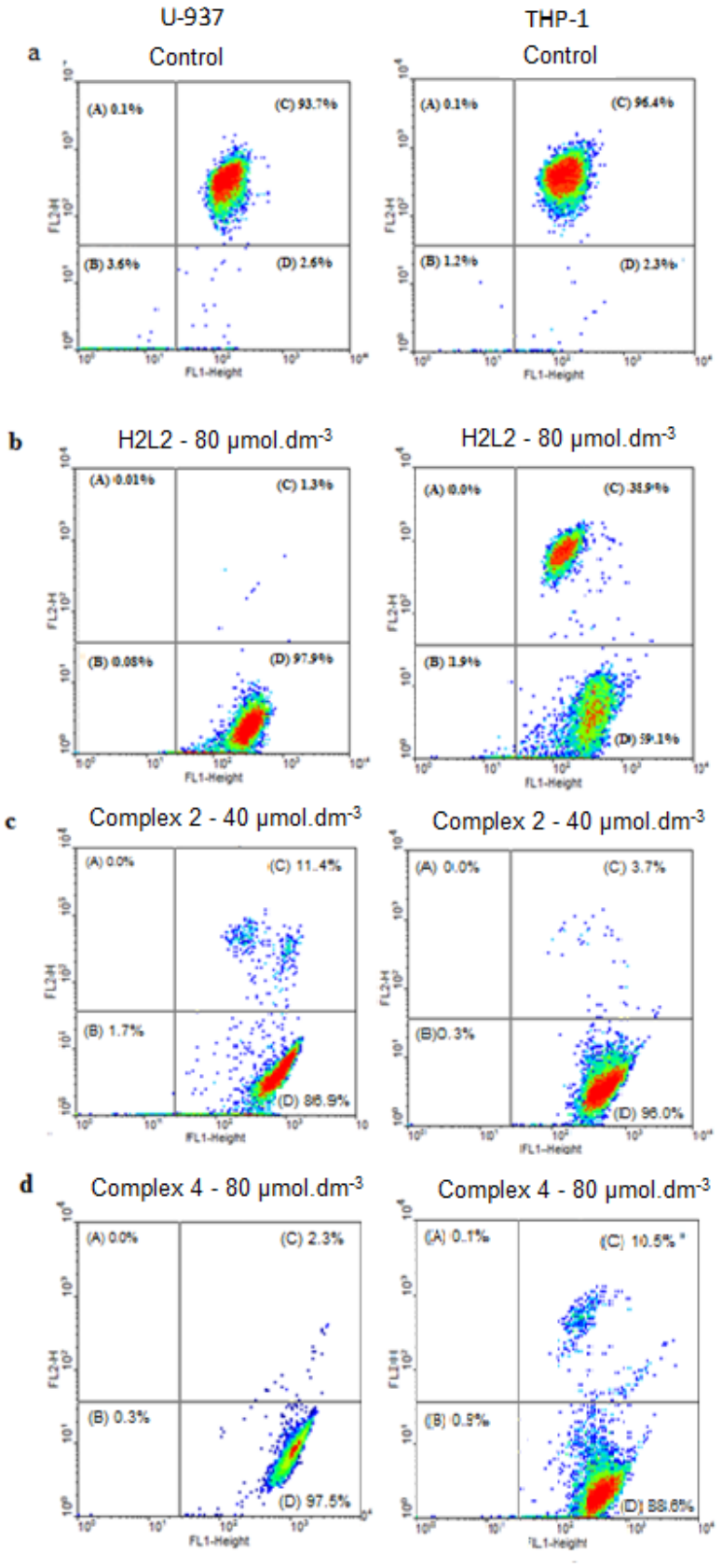

Figure 13. Mitochondrial transmembrane potential (ΔΨm) assay. THP-1 and U937 cell lines were incubated with H2L2 and complexes **(2)** and **(4)** for 36 h. After being stained with JC-1, cells were analyzed by flow cytometry. Quadrant C – Mitochondria containing red JC-1 aggregates in healthy cells are detectable in the FL2 channel. Quadrant D - Green JC-1 monomers in apoptotic cells are detectable in the FITC channel (FL1) and express a loss of ΔΨm. (a) Control cells; (b) Cells after treatment with 80 μmol dm^{-3} of H2L2; (c) cells after treatment with 40 μmol dm^{-3} of complex **(2)**; (d) cells after treatment with 80 μmol dm^{-3} of complex **(4)**.

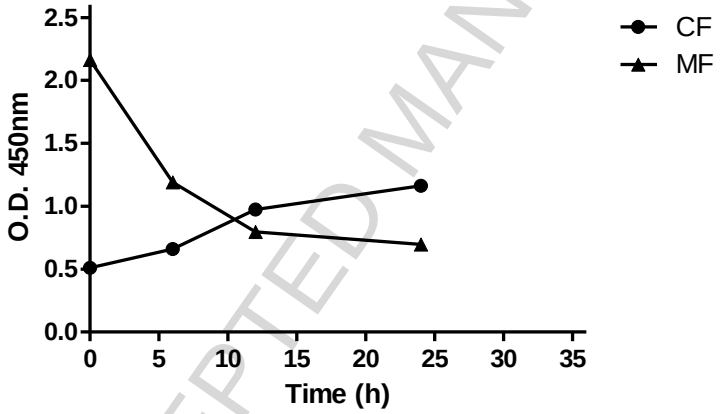

Figure 14. Time course of cytochrome *c* release in apoptotic U937 cells after treatment with complex **(2)**. Cells were incubated with complex **(2)**, at 40 μmol dm^{-3}, for 6, 12, and 24 h. After cell fractionation cytochrome *c* was quantified in both fractions according using the *Cytochrome c ELISA KIT* (Calbiochem®). CF – cytoplasmatic fraction, MF – mitochondrial fraction.

3.14. Analysis of mitochondrial morphology by fluorescence imaging and transmission electron microscopy (TEM).

To confirm if complex **(2)**-mediated loss of the mitochondrial membrane potential of U937 cells is related to morphological changes, the disruption of mitochondria was assessed by monitoring their morphology using fluorescence imaging and transmission electron microscopy (TEM) (Figure 15). As

shown in Figure 15B, mitochondrial swelling and disruption is evident after 12 h of incubation. The damage to the mitochondrial morphology appears to be dependent on the incubation time since it is considerably more noticeable after 24 h of incubation than after 12 h (Figure 15C). The TEM analysis furthermore shows greatly altered mitochondria (Figures 15B and 15C, bottom), with some of them having an empty matrix (indicated by arrows). Taken together, these data and the others presented above clearly show the mitochondrial impairment imposed by compound **(2)**, in agreement with the loss of the mitochondrial membrane potential ($\Delta\Psi m$).

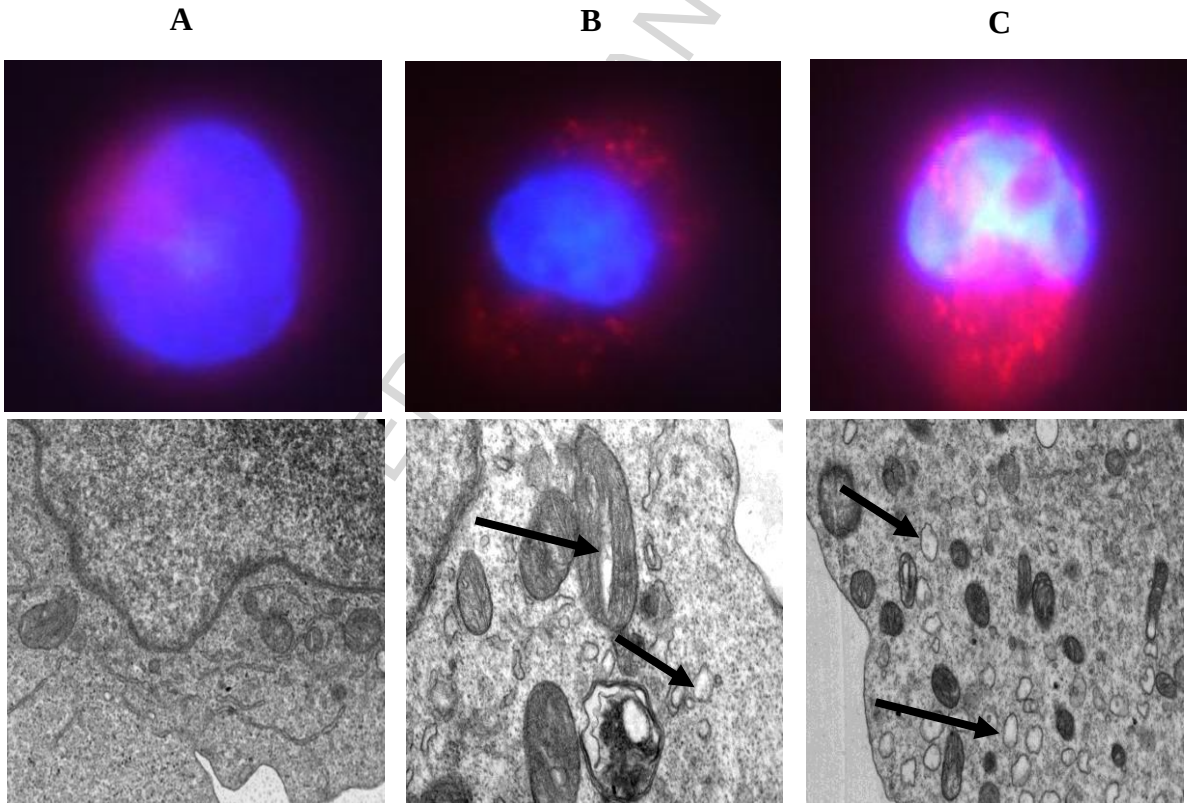

Figure 15. Visualization of mitochondrial disruption after 12 and 24 h of incubation with complex **(2)** (40 μmol dm^{-3}). Fluorescence imaging of the mitochondrial morphology with mitotracker and Hoechst nuclear staining (top), and transmission electron microscopy (bottom). (A) Control cells, (B) U937 cell line incubated with 40 μmol dm^{-3} of complex **(2)** for 12 h, (C) U937 cell line incubated with 40 μmol dm^{-3} of complex **(2)** for 24 h.

3.15. Determination of caspase activities.

Although it was shown above that the cells treated with the compounds show mitochondrial impairment, it is known that in mammalian cells the apoptotic response is mediated through either an intrinsic or extrinsic pathway, [52] involving caspases. Caspases are central components of the apoptotic response. They form a conserved family of enzymes that irreversibly commit a cell to die. Caspases are activated via an intrinsic or extrinsic pathway, distinguished by the initiator caspase that starts the activation cascade.[53]

The intrinsic pathway is mediated by mitochondria and, in response to apoptotic stimuli, several proteins are released from the intermembrane space of the mitochondria into the cytoplasm.[51] Some of the well-characterized proteins include cytochrome *c*, which is considered as a pro-apoptotic protein which binds to the protein APAF1. This interaction triggers a conformational change in APAF1 that then facilitates the formation of an apoptosome, which in turn mediates the activation of caspase-9 and other caspases.[54,55] In contrast, in the extrinsic pathway the most common initiator caspase would be caspase-8.

After the activation of the initiator caspase the activation of the effector caspase-3 is initiated. Furthermore, the activation of procaspase-9 requires the release of cytochrome *c* from the mitochondrial intermembrane space into the cytoplasm, where it forms a complex with procaspase-9, APAF1 and dATP.[56] The release of cytochrome *c* into the cytoplasm is thought to be the limiting factor in caspase-9 activation and the subsequent activation of caspase-3, an effect that was observed in this study. However, in the extrinsic pathways the initiator caspase-8 can directly activate caspase-3. Furthermore, caspase-8 activation can lead also to mitochondrial dysfunction, cytochrome *c* release and caspase-9 activation through cleavage of Bid.[57] Therefore, it is not possible to prove unequivocally that compound **(2)** is activating the intrinsic apoptotic pathway by only evaluating mitochondrial protein release. Therefore, in an attempt to clarify if cell death follows an intrinsic or extrinsic apoptotic

pathway we evaluated the activation of several caspases (2, 3, 4, 8, and 9).

As shown in Figure 14, release of cytochrome *c* from the mitochondria of the U937 cell line, after treatment with 40 μmol dm^{-3} complex **(2)**, was evident after 10 to 15 h of incubation; longer incubation periods did not lead to a significant further increase of cytosolic cytochrome *c*. Based on this observation we hypothesize that caspase-9 may be fully activated after 15 h. Figure 16A shows that complex **(2)** activates both initiator caspases and the effector caspase-3, as demonstrated by a comparison with untreated control cells (0 h sample). However, a significant rise in caspase-9 activity is observed only after 12 h of incubation, while caspase-8 activity starts earlier and increases more gradually. These results are in agreement with the cytochrome *c* release assay (Figure 14) and indicate that caspase-9 is activated right after cytochrome *c* release from the mitochondria. Interestingly, these results also suggest that caspase-8 is upstream of caspase-9 since it is activated earlier. Thus, the apoptosis signal is started by the extrinsic pathway and amplified subsequently by the mitochondria. Furthermore, caspase-3 is activated earlier than caspase-9, also indicating that the extrinsic pathway is being activated before the intrinsic one, through caspase-8 activation. This hypothesis may be substantiated further by the presence of caspase-4 (another caspase of the death receptor pathway) in the early phase following the addition of complex **(2)**. Caspase-4 can be activated by death receptors and trigger the endoplasmic reticulum to release calcium ions (Ca^{2+}) into the cytosol.[58] This increase triggers other chemical changes, including the release of more cytochrome *c* from mitochondria, which induce apoptosis. Caspase-2 is activated earlier than caspase-9, indicating that it could be acting as an apical caspase. Recently, Jelínk and co-workers reported a key role of caspase-2 in main death-inducing pathway after taxane application in tested breast cancer cells.[59] Caspase-2 is universal following apoptosis signaling by either mitochondrial or death receptor pathway.[60]

We performed the same experiment with cisplatin. Similar to the experiments with complex **(2)**, cytochrome *c* release after treatment with cisplatin initiates activation of several of the signaling

caspases (caspases 2, 3, 8 and 9, as well as effector caspase-3). However, in contrast to the incubation with complex **(2)**, no significant activity of caspase-4 was detected, even after 12 h. These results strongly suggest that cisplatin induces apoptosis in U937 cells mainly *via* the mitochondrial pathway. On the other hand, the apoptosis signal triggered by complex **(2)** appears to start from the extrinsic pathway with activation of caspases 4 and 8, and this signal is amplified by the mitochondria with the concomitant release of cytochrome *c* and caspase-9 activation.

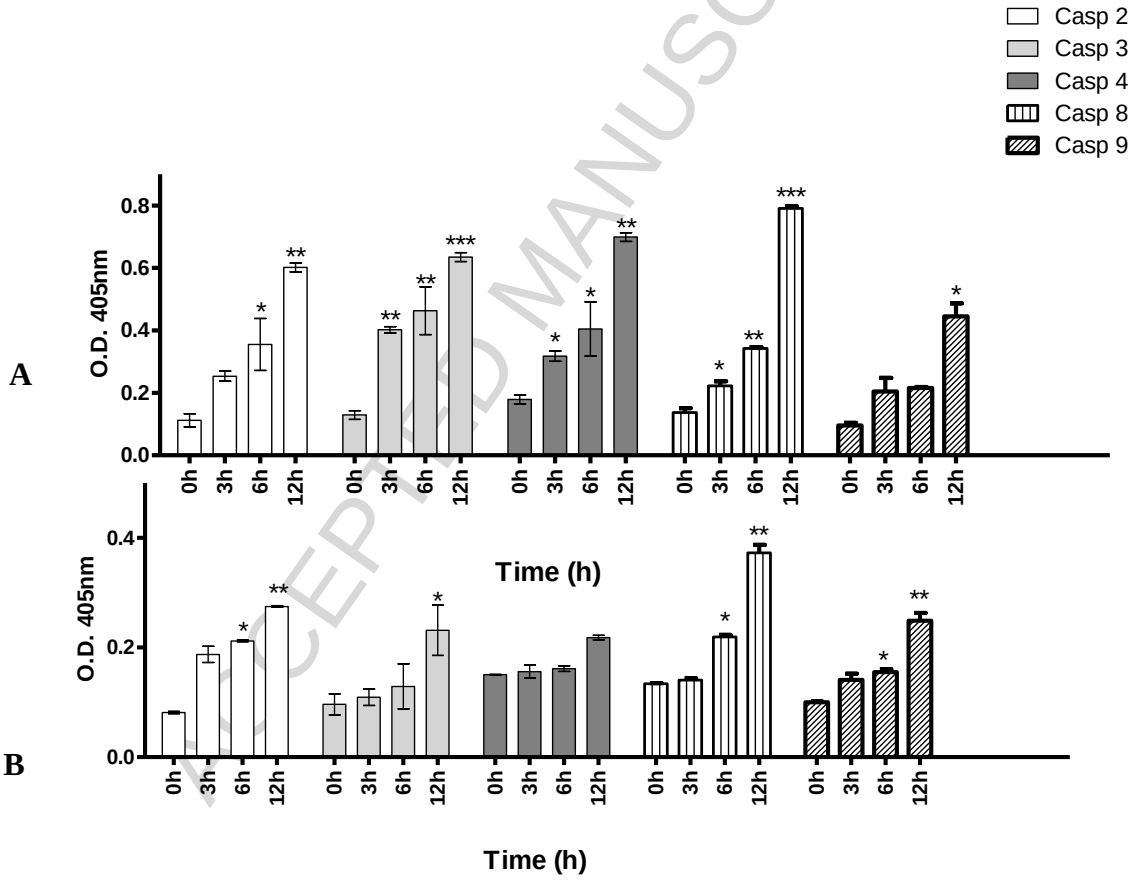

Figure 16. Activation assays of caspases 2, 3, 4, 8 and 9 employing the U937 cell line. Cells were incubated with 40 μmol dm^{-3} of complex **(2)** (A) or 50 μmol dm^{-3} of cisplatin (B) for 3, 6 and 12 h (0 h –untreated control cells). Caspase activities were determined using the *ApoTarget*™ caspase colorimetric protease assay kit (Invitrogen™). Values are means ± SD from two separate measurements. **P* < 0.05, ***P* < 0,01 and ****P* < 0,001 *versus* control.

We have previously reported that during the initial stage of the treatment of leukemia cell line U937 with the complex [Cl(HPClNOL)Fe(μ-O)Fe(HPClNOL)Cl]Cl_2.2H_2O mitochondria lose their transmembrane potential, resulting in cytochrome *c* release. The quantification of caspases 3, 8 and 9 indicated that both the intrinsic (*via* mitochondria) and extrinsic (*via* death receptors) pathways were involved in the apoptotic stimuli.[20] Although this dinuclear iron(III) complex induces cell death by both pathways, it was only moderately active against U-937 cell line (IC_{50}= 86±1 μM).

Lou and co-workers reported that the copper complex [Cu(5-Cl-pap)(OAc)(H_2O)].2H_2O presents a potent antiproliferative effect in human breast cancer cell line MCF-7, with IC_{50} values comparable to cisplatin. This antitumor mechanism of action might be via mitochondrial pathway, by the activation of caspase-9 and capase-3.[61]

As shown above, the induction of apoptosis by compound **(2)** clearly starts with the caspase-8 activation, which suggests that death receptors in the cell wall are the first target. This feature is a very important aspect related to compound **(2)** activity, which does not need to enter into the cell to induce the apoptotic signaling. Thus, our results indicate that the development of compounds that target death receptors in the cell wall, thus activating the extrinsic apoptotic pathway, may be an interesting strategy to improve the efficacy of future anticancer agents.

4. Conclusions

In this study we have introduced four new ligands and their copper complexes. The physico-chemical characterization showed that the compounds have a dinuclear structure in the solid state, which is broken in solution, resulting in mononuclear copper complexes.

The insertion of the naphthyl group into the ligand was an attempt to develop copper complexes with high anticancer activity. In the present family of copper complexes we observed that those which contain the phenol group (complexes **(2)** and **(4)**) are more efficient than those lacking this unit

(complexes **(1)** and **(3)**). Furthermore, we observed that the complexes containing the α-naphthyl unit are more active than those containing the β-naphthyl isomer, highlighting the relevance of the substitution on the naphthalene ring to anticancer activity.

All the tested compounds induce the death of cancer cells. Compound **(2)** was the most efficient, having an IC_{50} value similar to that of cisplatin for THP-1 cells, and even better than cisplatin for U937 cells. However, **(2)** was more toxic to normal cells (PBMC) than cisplatin. This would indicate a drawback for its future application, but fortunately, this behavior was not observed in *in vivo* tests where compound **(2)** appeared safer than cisplatin.

A large number of techniques (fluorescence microscopy, annexin V assay, cycle arrest, mitochondrial membrane potential and cytochrome C release, transmission electron microscopy) confirm that compound **(2)** induces apoptosis in cancer cells and the impairment of mitochondria since both the loss of membrane potential and cytochrome *c* release was observed. However, mitochondria are not the first target for compound **(2)** since caspase-8 is activated first, promoting the subsequent caspase-3 (effector) activation, which leads to an impairment of mitochondria and the concomitant enhancement of the apoptotic signal. This result is of great relevance since caspase-8 activation promoted by compound **(2)** indicates the interaction of this compound with death receptors on the cell wall, suggesting that compound **(2)** does not need to enter the cancer cells to kill them. This mode of action is fortuitous since there is no problem associated with drug uptake, as is commonly observed for cisplatin. Therefore, death receptors are an interesting target for the development of anticancer drugs.

Based on these encouraging results, further studies are planned with these compounds against colon, liver and prostate cell lines in views of the limited therapeutic options for cancers affecting those tissues. Furthermore, some *in vivo* studies are currently in progress.

5- Abbreviations

ΔΨm: mitochondrial membrane potential

EDTA: Ethylenediaminetetraacetic acid

H_2BPClNOL (= 1-(bis-pyridin-2-ylmethyl-amino)-3-chloropropan-2-ol)

HPClNOL= [1-(bis-pyridin-2-ylmethyl-amino)-3-chloropropan-2-ol)

LD_{50}: Standard measure of the toxicity of a material that will kill half of the sample population of a specific test animal in a specified period through exposure via ingestion, skin contact, or injection.

MTT: 3-(4,5-dimathylthiazol-2-yl)-2,5- diphenyltetrazolium bromide

PBMC: peripherical blood mononuclear cell

PBS: phosphate buffer saline

PI: propidium iodide

TEM: transmission electron microscopy

THP-1: Human monocytic cell line derived from an acute monocytic leukemia patient

TRIS: tris(hydroxymethyl)aminomethane

U937: Human cell line established from a diffuse histiocytic lymphoma and displaying many monocytic characteristics

Acknowledgements

The authors are grateful to financial support received from CAPES (Coordenação de Aperfeiçoamento de Pessoal de Nível Superior), CNPq (Conselho Nacional de Desenvolvimento Científico e Tecnológico) FAPERJ (Fundação de Amparo à Pesquisa do Estado do Rio de Janeiro) and FINEP (Financiadora de Estudos e Projetos). G. S. also acknowledges the receipt of an ARC Future Fellowship (FT120100694).

Appendix A. Supplementary data

Figures 1S-6S, in PDF format. Crystallographic data (without structure factors) for the structure reported in this paper have been deposited with the Cambridge Crystallographic Data Centre as supplementary publication: deposition number: CCDC 913726 for complex **(2)** and CCDC 1055915 for complex **(4)**. Copies of the data can be obtained free of charge from the CCDC (12 Union Road, Cambridge CB2 1EZ, U.K.; phone: (+44) 223-336-408; fax: (+44)1223-336-003; e-mail: deposit@ccdc.cam.ac.uk; Web site www.ccdc.cam.ac.uk

References

[1] www.lls.org/diseaseinformation- Leukemia & lymphoma society.

[2] R. Willemze, S. Suciu, G. Meloni, B. Labar, J. P. Marie, C. J. Halkes, P. Muus, M. Mistrik, S. Amadori, G. Specchia, F. Fabbiano, F. Nobile, M. Sborgia, A. Camera, D. L. Selleslag, F. S. Lefrère, D. Magro, S. Sica, N. Cantore, M. Beksac, Z. Berneman, X. Thomas, L. Melillo,J. E. Guimaraes, P. Leoni, M. Luppi, M. E. Mitra, D. Bron, G. Fillet, E. W. Marijt, A. Venditti, A. Hagemeijer, M. Mancini, J. Jansen, D. Cilloni, L. Meert, P. Fazi, M.Vignetti, S. M. Trisolini, F. Mandelli and T. de Witte, *J. Clin. Oncol.,* 2014, **32(3)**, 219-228.

[3] E. C. Attar , J. L. Johnson, P.C. Amrein, G. Lozanski, M. Wadleigh, D. J. DeAngelo, J. E. Kolitz, B. L. Powell, P. Voorhees, E. S. Wang, W. Blum, R. M. Stone, G. Marcucci, C. D. Bloomfield,B. Moser and R. A. Larson, *J. Clin. Oncol.* 2013, **31(7)**, 923-929.

[4] S. K.Tasian1, J. A. Pollard and R. Aplenc, *Front. Oncol.,* 2014, **4**, 1-11.

[5] D.Ksienski, *Clin. Med. Insights. Oncol,.* 2011, 5, 369-379.

[6] K. Vandyke, S. Fitter and A. C. W. Zannettino, *Blood Cancer Journal*, 2011, 1-4.

[7] N. K. Y. Wee, D. C. Weinstein, S. T. Fraser and S. J. Assinder, *Int. J. Biochem. Cell. Biol.,* 2013, **45**, 960-963.

[8] W. Zhou, X. Wang, M. Hu, C. Zhu and Z. Guo, *Chem. Sci.*, 2014, **5**, 27612769.

[9] M. Li, T. Lan, X. Cao, H. Yang, Y. Shi, C. Yi and G. Chen, *Dalton Trans.*, 2014, **43**, 2789-2798.

[10] G. Barone, A. Terenzi, A. Lauria, A. M. Almerico, J. M. Leal, N. Busto and B. Garcia. *Coord. Chem. Rev.,* 2013, **257**, 2848-2862.

[11] D. Palanimuth, S. V. Shinde, K. Somasundaram and A. G. Samuelson, *J. Med. Chem.,* 2013, **56(3)**, 722-734.

[12] W. Wather, I. Fichtner, F, Hackenberg, W. Strieciwilk and M. Tacke, *Lett. Drug Des. Discovery,* 2014, **11(7)**, 825-832.

[13] V. Gandin, F. Tisato, A. Dolmella, M. Pellei, C. Santini, M. Giorgetti, C. Marzano and M. Porchia. *J. Med. Chem.*, 2014, **57**, 4745-4760.

[14] P. Martinez-Bulit, A. Garcia-Ortíz, E. Mijangos, L. Barrón-Sosa, F. Sánchez-Bartiz, I. Gracia-Mora, A. Flores-Parra, R. Contreras, J. Reedijk and N. Barba-Behrens. *J. Inorg. Biochem.*, **142**, 2015, 1-7.

[15] R. Safi, E. R. Nelson, S. K. Chitneni, K. J. Franz, D. J. George, M. R. Zalutsky and D. P. McDonnell, *Cancer Res.*, 2014, **74(20)**, 5819-5831.

[16] J. Zha, F. Chen, H. Dong, P. Shi, Y. Yao, Y. Zhnag, R. Li, S. Wang, P. Li, W. Wang and B. Xu, *J. Transl. Med.,* 2014 **(12)** 163-171.

[17] D. Montagner, V. Gandin, C. Marzano and A. Erxleben. *J. Inorg. Biochem.*, 2015 **(145)** 101-107

[18] T. Ma, J. Xu, Y. Wang, H. Yu, Y.Yang, Y. Liu, W. Ding, W. Zhu, R. Chen, Z. Ge, Y. Tan, L. Jia and T. Zhu. *J. Inorg. Biochem.,* 2015 **(144)** 38-46.

[19] C. Fernandes, G. L. Parrilha, J. A. Lessa, L. J. M. Santiago, M. M. Kanashiro, F. S. Boniolo, A. J. Bortoluzzi, N. V. Vugman, M. H. Herbst and A. Horn, Jr. *Inorg. Chim. Acta.*, 2006, **359**, 3167-3176.

[20] A. Horn Jr, C. Fernandes, G. L. Parrilha, M. M. Kanashiro, F. V. Borges, E. J T. de Melo, G. Schenk, H. Terenzi and C. T. Pich, *J. Inorg. Biochem.*, 2013, **128**, 38-47.

[21] T. P. Ribeiro, C. Fernandes, K. V. Melo, S. S. Ferreira, J. A. Lessa, R. W. A. Franco, G. Schenk. M. D. Pereira and A. Horn Jr, *Free Radic. Biol. Med.,* 2015, **80**, 67-76.

[22] Constantino et al. *Intensive Care Med. Exp.,* 2014, 2:17.

[23] C. Fernandes, A. Horn Jr, O. Vieira-da-Motta, V. M. de Assis, M. R. Rocha, L. S. Mathias, E. S. Bull, A. J. Bortoluzzi, E. N. Guimarães, J. C. A. de Almeida and D. H. Russell. *J. Inorg. Biochem.,* 2010, **104**, 1214-1233.

[24] H. N. Chopade, *Chem. Tech.,* 2010, **2**, 1823-1830.

[25] B. Das, C. R. Reddy, J. Kashanna, S. K. Mamidyala and C. G. Kumar, *Med. Chem. Res,*. 2012, **21**, 3321-3325.

[26] A. M. Maurice. Acquisition of anisotropic information by computational analysis of isotropic EPR spectra. PhD thesis, University of Illinois, Urbana, Ill., 1980; M. J. Nilges. PhD thesis, University of Illinois, Urbana, Ill., 1979.

[27] Bruker APEX2, SAINT and SADABS, version 2011.8-0; Bruker AXS Inc., Madison, Wisconsin, USA

[28] G. M. Sheldrick, *Acta Cryst*., 2008. **A64**, 112-122 .

[29] A. L. Spek, *Acta Cryst.,* 2009, **D65**, 148-155.

[30] R. R. Gagné. C. A. Koval and G. C. Lisensky, *Inorg. Chem.,* 1980, **19**, 2854-2855.

[31] A. Neves, M.A. de Brito, V. Drago, K. Griesar and W. Haase, *Inorg. Chim. Acta.,* 1995, 237, 131-135.

[32] A. Neves, M.A. de Brito, I. Vencato, V. Drago, K. Griesar, W. Haase and Y. P. Mascarenhas, *Inorg. Chim. Acta.,* 1993, 214, 5-8.

[33] B. Kosmider, E. Zyner, R. Osiecka and J. Ochok, *Mutat Res.,* 2004, **563**, 61-70.

[34] Software GraphPad Prism Versão 5.0.

[35] C. Fernandes, R. O. Moreira, L. M. Lube, A. Horn Jr., B. Szpoganicz, S. Sherrod and D. H. Russell, *Dalton Trans.,* 2010, **39**, 5094-5100.

[36] C. J. Williams, H. Morris, J. Svorec, M. Valkova, M. Valko, J. Moncol, M. Mazur, F. Valach and M. Melnik, *J. Mol. Struct.,* 2003, **659**, 53-60.

[37] T. G. V. M. Rao, A. R., Kumar, C. K. Chakravarthi, M. R. Reddy and N. Veeraiah, *Physica B.,* 2012, **407**, 593-597.

[38]. M. Brustolon, E. Giamello, Electron Paramagnetic Resonance: A practitioner´s toolkit, Wiley, 2009.

[39] K. Kivelson and R. Nieman, *J. Chem. Phys.*, 1961, **35**, 149-155.

[40] E. Kalfaoglu and B. Karabulut, *Chem. Phys.Let.,* 2011, **505**, 154-156.

[41] L. L. Mendes, C. Fernandes, R. W. A, Franco, L. M. Lube, S. Wei, J. H. Reibenspies, D. J. Darensbourg and A. Horn Jr. *J. Braz. Chem. Soc.,* 2014, **25**, 1050-1061.

[42] M.C. Esmelindro, E. G. Oestreicher, M. Caovilla, J. A. Lessa, C. Fernandes, C. Dariva. S. M. Egues. A. J. Bortoluzzi and O.A. C. Antunes, *J. Braz. Chem. Soc.*,2006, **17**, 1551-1557.

[43] A. Ghadersohi, D. Pan, Z. Fayazi, D. G. Hicks, J. S. Winston and F. Z. Li. *Breast Cancer Res. Treat.,* 2007, **102**, 19-30.

[44] a) F. Bisceglie, S. Pinelli, R. Alinovi, P. Tarasconi, A. Buschini, F. Mussi, A. Mutti and G. Pelosi. *J. Inorg. Biochem.,* 2012, **116**, 195-203.b) L. Garcia, S. Franzoni, F. Mussi, M. A. Niçaise, H. Bertrand, M. Desmadril, G. Pelosi, A. Buschini and C. Policar. *J. Inorg. Biochem.,* 2014, **135**, 40-44. c) M. Trendowski, V. Wong, G. Yu and T. P. Fondy. *Anticancer Res.,* 2015, **35**, 65-76.

[45] a) A. D. Garg, D. Nowis, J. Golab, P. Vandenabeele, D. V. Krysko and P. Agostinis. *Biochim. Biophys. Acta.,* 2010, **1805**, 53-71. b) C. M. Walsh, *Front. Cell Dev. Biol.,* 2014, 1-4.

[46] S. Elmore. *Toxixol. Pathol.,* 2007, **35(4)**, 495-516.

[47] X. Yan and R. A. Gemeinhart, *J. Control. Release*., 2005, **106**, 198-208.

[48] M. Barceló-Oliver, Á. Garcia-Raso, Á. Terrón, E. Molins, M. J. Prieto, V. Moreno, J. Martínez, V. Lladó, I. López, A. Gutiérrez, P. V. Escibá, *J. Inorg. Biochem.,* 2007, **101**, 6490-659.

[49] Z-Ying Ma, X. Qiao, C-Zhi Xie, J. Shao, J-Yuan Xu, Z-Yan Qiang and J-Shi Lou, *J. Inorg. Biochem.,* 2012, **117**, 1-9.

[50] D. R. Green and J. C. Reed, *Science.,* 1998, **281**, 1309-1212.

[51] A. Perelman, C. Wachte, M. Cohen, S. Haupt, H. Shapiro and A. Tzur, Cell Death and Disease, 2012, **3**, 1-7.

[52] J. Yuan, *Curr. Opin. Cell. Biol.,* 1997, **9**, 247-251.

[53] J. E. Chipuk, *Mol.Cell.,* 2010, **37**, 299-310.

[54] X. Jiang and X. Wang, *J. Biol. Chem.,* 2000, **275**, 31199-31203.

[55] G. Evan and T. Littlewood, *Science.,* 1998, **281**, 1317-1322.

[56] D. Xue, S. Shaham and H. R. Horvitz, *Genes Dev.,* 1996, **10**, 1073-1083.

[57] K. B. Elkon, *J. Exp. Med.,* 1999, **190**, 1725-1728.

[58] X. Luo, I. Budihardjo, H. Zou, C. Slaughter and X. Wang, X. *Cell.,* 1998, **94**, 481–490, 1998.

[59] M. Jelínk et al. *Cancer Cell Int.,* 2015, **15**, 2-16.

[60] S. Kumar. *Nat. Rev. Cancer.,* 2009, **9**, 897-903.

[61] Z.-Y. Ma, X. Qiao, C.-Z. Xie, J. Shao, J.-Y.Xu, Z.-Y. Qiang and J.-S.Lou. *J. Inorg. Biochem.,* 2012, **117**, 1-9.

Graphical abstract

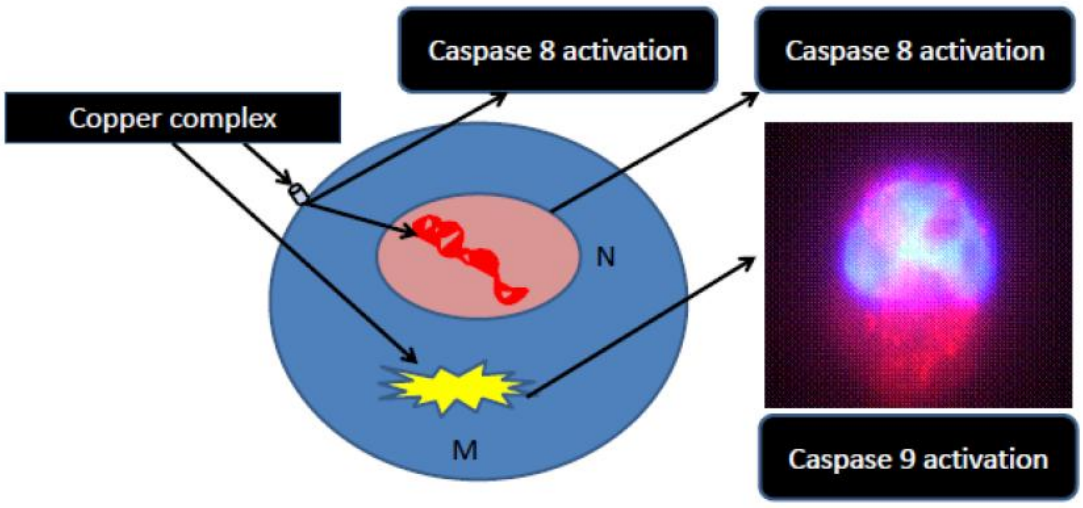

Synopsis

In this paper we present the synthesis, physico-chemical properties and cytotoxicity toward two human leucemia cell lines of four new copper(II) complexes. Complex (2) showed relevant antiproliferative effect against both cell lines and the mechanism of action starts from an extrinsic pathway and is amplified by the mitochondria.

Highlights:

- New copper(II) complexes containing naphthalene rings (*alpha* and *beta*);
- X-ray diffractions studies and several investigations in solution were performed;
- Complex **(2)** is almost four times less toxic than cisplatin, based on LD_{50} values;
- Complex **(2)** exhibits higher activitity than cisplatin against U937;
- 5-The apoptosis signal triggered by complex **(2)** starts from an extrinsic pathway.